Architectonic Mapping of Somatosensory Areas Involved in Skilled Forelimb Movements and Tool Use

Andrei Mayer,[1] Márcio L. Nascimento-Silva,[1] Natalia B. Keher,[1] Ruben Ernesto Bittencourt-Navarrete,[2] Ricardo Gattass,[1] and João G. Franca[1]*

[1]Institute of Biophysics Carlos Chagas Filho, Federal University of Rio de Janeiro, Rio de Janeiro, Brazil
[2]Department of Physiology, Institute of Biological Science, Federal University of Juiz de Fora, Juiz de Fora, Brazil

Cebus monkeys stand out from other New World monkeys by their ability to perform fine hand movements, and by their spontaneous use of tools in the wild. Those behaviors rely on the integration of somatosensory information, which occurs in different areas of the parietal cortex. Although a few studies have examined and parceled the somatosensory areas of the cebus monkey, mainly using electrophysiological criteria, very little is known about its anatomical organization. In this study we used SMI-32 immunohistochemistry, myelin, and Nissl stains to characterize the architecture of the parietal cortical areas of cebus monkeys. Seven cortical areas were identified between the precentral gyrus and the anterior bank of the intraparietal sulcus. Except for areas 3a and 3b, distinction between different somatosensory areas was more evident in myelin-stained sections and SMI-32 immunohistochemistry than in Nissl stain, especially for area 2 and subdivisions of area 5. Our results show that cebus monkeys have a relatively complex somatosensory cortex, similar to that of macaques and humans. This suggests that, during primate evolution, the emergence of new somatosensory areas underpinned complex manual behaviors in most Old World simians and in the New World cebus monkey. J. Comp. Neurol. 524:1399–1423, 2016.

INDEXING TERMS: parietal cortex; somatosensory cortex; cebus monkey; area 5; RRID:AB_509998; RRID: nif-0000-10294

The ability to perform skilled hand movements and to manipulate tools are landmarks in primate evolution. They allow individuals to accurately interact with and modify the external environment in accordance with their needs. The importance of these behaviors can be readily appreciated when we think about our daily activities. Almost everything we do is achieved by the use of our hands and tools, as when we type in a keyboard, peel a fruit, or open a wallet. Correct performance of such trivial tasks depends on different sectors of the parietal cortex that process and integrate somatosensory inputs from the forelimbs.

Accordingly, macaque monkeys are skilled (Malaivijitnond et al., 2007; Gumert et al., 2009; Gumert and Malaivijitnond, 2013) and present a relatively complex somatosensory cortex, composed of a number of different areas similar to that of humans (Geyer et al., 1997; Scheperjans et al., 2005). Brodmann (1909) used Nissl-stained sections to parcel the primate somatosensory cortex into four architectonic areas, 3, 1, 2, and 5. Currently, based especially on cytoarchitectural and electrophysiological data, there is a general agreement that area 3 of Brodmann is actually composed of two different areas, 3a and 3b, and that area 5 can also be further subdivided into at least two different architectonic sectors (Pandya and Seltzer, 1982; Lewis and Van Essen, 2000; Bakola et al., 2010, 2013). However, the architectonic organization of somatosensory areas is still not well established. After the pioneer cytoarchitectonic studies (Brodmann, 1909; Vogt and Vogt, 1919; von Economo and Koskinas, 1925; von Bonin and Bailey, 1947; Powell and Mountcastle, 1959), little attention has been given to the architectonic organization of parietal areas in macaque monkeys. The architectonic

Grant sponsor: Conselho Nacional de Desenvolvimento Científico e Tecnológico (CNPq-Brasil); Grant sponsor: Fundação Carlos Chagas Filho de Amparo à Pesquisa do Estado do Rio de Janeiro (FAPERJ).

*CORRESPONDENCE TO: Dr. João G. Franca, Centro de Ciências da Saúde, Instituto de Biofísica Carlos Chagas Filho, Universidade Federal do Rio de Janeiro, Avenida Carlos Chagas Filho, 373, Bloco G - 1° andar- Sala G1-019, Cidade Universitária – Ilha do Fundão, 21941-902 Rio de Janeiro, Brazil. E-mail: jgfranca@biof.ufrj.br

Received September 11, 2014; Revised October 13, 2015;
Accepted October 15, 2015.
DOI 10.1002/cne.23916
Published online November 23, 2015 in Wiley Online Library (wileyonlinelibrary.com)

data available in the literature of the past few decades are complementary to electrophysiological and/or connectivity studies (Jones et al., 1978; Nelson et al., 1980; Pons et al., 1985; Krubitzer et al., 2004; Breveglieri et al., 2006; Gharbawie et al., 2011; Seelke et al., 2012; Bakola et al., 2013). Occasionally, architectonic data are not even shown, as in the case of the myeloarchitecture of area 5 described by Pandya and Seltzer (1982). Furthermore, except for two more recent studies (Lewis et al., 1999; Lewis and Van Essen, 2000), the anatomical characterization of parietal areas was focused mostly on the cytoarchitecture revealed by Nissl-stained sections (Powell and Mountcastle, 1959; Nelson et al., 1980; Pandya and Seltzer, 1982; Pons et al., 1985; Krubitzer et al., 2004), but the characterization by other more recently developed techniques, such as SMI-32 immunohistochemistry (Campbell and Morrison, 1989), has been neglected. Although the boundaries between areas 3a, 3b, and 1 are clear in Nissl-stained sections (Powell and Mountcastle, 1959; Nelson et al., 1980), the limits of areas 2 and 5, as well as their anatomical subdivisions, are not evident based on cytoarchitecture alone (Powell and Mountcastle, 1959; Jones et al., 1978; Lewis et al., 1999). Some studies have examined areas 2 and 5 of macaques also using myelin stain and SMI-32 immunohistochemistry (Lewis et al., 1999; Lewis and Van Essen, 2000), but in the case of area 5, just a brief description of its subdivisions has been provided.

In the present study we used SMI-32 immunohistochemistry, in addition to Nissl and myelin stains, to examine the architectonic organization of the somatosensory cortex in the New World cebus monkey. These animals stand out from other New World monkeys and even from macaques by their manual abilities and tool use behaviors. Cebus monkeys can execute 16 different types of precision grip, including the opposition of the thumb and the index finger (Spinozzi et al., 2004, 2007). In the wild, they use rocks as hammers and anvils (Moura and Lee, 2004), and select the best tool for a specific task, based on its physical properties (Visalberghi et al., 2009; Manrique et al., 2011). They manufacture tools, e.g., by shaping sticks as insect-probing tools (Mannu and Ottoni, 2009). Therefore, cebus monkeys are great models for the study of the neural basis of manual behaviors and tool use. Based on behavioral data, one could hypothesize that cebus monkeys have a parietal cortex at least as developed as that of macaque monkeys. For instance, Padberg et al. (2007) presented electrophysiological evidence that cebus monkeys, in contrast to other New World monkeys possess an area 2 and a well-developed area 5, similar to Old World monkeys (macaques). However, like in macaque monkeys, the architectonic organization of the somatosensory cortex of cebus monkeys is still poorly characterized. In this study we aimed to describe the organization of the somatosensory cortex of the cebus monkey, using different anatomical processing techniques and determining which adequately identifies anatomical borders between different parietal areas.

MATERIALS AND METHODS

In this study we used eight adult cebus monkeys (*Sapajus* s.p., formerly known as *Cebus* s.p.) of both sexes weighing between 2.4 and 4.4 kg. Animals were obtained from the animal facility of the Institute of Biophysics Carlos Chagas Filho (IBCCF), under the license of the Brazilian Institute of the Environment and Renewable Natural Resources (IBAMA). All experimental procedures were approved by the local animal care and use committee (CEUA-CCS/UFRJ, protocol #IBCCF-119) and are in accordance with Brazilian Law and the guidelines published in the NIH *Guide for Care and Use of Laboratory Animals* (http:www.nap.edu/catalog/12910.html). Six animals used in this study (of a total of eight) underwent two surgical procedures separated by an interval of 7 to 14 days for a related study. In the first session, a brief electrophysiological recording was made to guide injections of neuroanatomical tracers in the parietal cortex. In the second session, somatosensory mapping around the tip of the intraparietal sulcus (IPS) was performed for physiological identification of the approximate border between areas 2 and 7b. The cortices of two additional animals (CB78 and V2-02) were obtained from unrelated studies in which only the occipital pole was surgically exposed.

Electrophysiological recording

Animals were initially anesthetized with intramuscular injections of ketamine hydrochloride (15 mg/kg) and xylazine (1 mg/kg), and then administered atropine (0.04 mg/kg), diazepam (1.3 mg/kg), and dexamethasone (0.4 mg/kg). Surgical levels of anesthesia were maintained with supplemental doses of ketamine and xylazine (5:1) delivered intramuscularly. Throughout the experiment, temperature, heart, and respiration rates were monitored. Once deeply anesthetized, the animals were placed in a stereotaxic frame, the skin was cut, the temporalis muscle was retracted, and a craniotomy was made over the parietal cortex. The dura mater over the exposed cortex was sectioned and the resulting flaps were retracted. A digital image of the exposed neocortex was made with an 8-Mp Canon SX100 camera. Electrophysiological recording sites were then

marked in this picture using the superficial blood vessels of the brain as landmarks.

Electrophysiological recordings were obtained with varnish-coated tungsten microelectrodes (0.5–0.6 MΩ at 100 Hz; Frederick Haer, Brunswick, ME; Micro Probe, Garden Grove, CA). The electrode was placed in an acrylic holder sustained by a stereotaxically guided micromanipulator. The manipulator was positioned in a way to allow perpendicular penetrations of the electrode into the cortical surface. The electrode was lowered into the cortex, until a depth of 500–1000 μm below the pial surface. Once the electrode was in place the body surface was stimulated and the multiunit receptive field at that cortical site was drawn on a diagram of the monkey body. The neural response was amplified, filtered, and monitored through a loudspeaker. We classified the intensity and the types of responses (i.e., as "cutaneous" or "deep"), according to the criteria described by Padberg et al. (2007). Cutaneous responses were elicited by light touch of the skin with a fine probe and/or by light brushing of hairs and skin. Deep responses were characterized by more vigorous squeezing of the hand or limb, by tapping over the skin, or by joint manipulation. Sulci pattern and tracer injection sites allowed us to relate recording sites to histologically processed tissue.

Histological processing

At the end of the electrophysiological mapping session, a lethal dose of sodium pentobarbitone (50 mg/kg) was administered intravenously. Animals were then transcardially perfused with 0.9% saline followed by 4% paraformaldehyde in phosphate buffer (pH 7.3), 4% paraformaldehyde in 2.5% sucrose phosphate buffer, 4% paraformaldehyde in 5% sucrose phosphate buffer, and then by 10% sucrose phosphate buffer, pH 7.2–7.4. The brain was removed from the skull and placed in a postfixation solution of 4% paraformaldehyde in 30% sucrose. Both hemispheres of each case were sectioned parasagittally, coronally, or horizontally at 40 or 50 μm. Adjacent sections were collected in 5 or 6 series for different histological processing protocols. In all cases, one of these series of sections was stained for Nissl substance (with cresyl violet). In two cases, one of the histological series was processed for myelin with the Gallyas (1979) or Heidenhain method (after Hutchins and Weber, 1983), and/or immunoreacted for neurofilaments (SMI-32 monoclonal antibodies; Sternberger and Sternberger, 1983; Campbell and Morrison, 1989).

SMI-32 immunohistochemistry

The SMI-32 monoclonal antibody (SMI 32, Covance Research Products, Denver, PA; Cat. no. SMI-32R-500, RRID:AB_509998) is a mouse monoclonal IgG1 that reacts with a nonphosphorylated epitope in neurofilament H of mammalian species. The reaction is masked when the epitope is phosphorylated and staining of isolated neurofilament preparations is greatly intensified upon dephosphorylation (Sternberger and Sternberger, 1983). It has been shown to be a very useful histological tool for cortical parcellation in different mammalian groups, including rodents (Boire et al., 2005; Van der Gucht et al., 2007; Dias et al., 2014) and primates (see below). Similar to macaques (Campbell and Morrison, 1989; Hof and Morrison, 1995; Lewis et al., 1999; Lewis and Van Essen, 2000), SMI-32 immunohistochemistry in the cebus monkey reveals a heterogeneous labeling pattern in the cortex (Soares et al., 2008; Cruz-Rizzolo et al., 2011) where two bands with varying levels of SMI-32 immunoreactivity are usually observed over layers III and V. These two bands are composed of small to large pyramidal neurons, including their proximal processes and fragments of apical dendrites.

In order to reveal SMI-32 immunoreactivity, free-floating sections were initially washed three times in phosphate buffer-saline (PBS) 0.1 M for 10 minutes, and subsequently incubated with 2% bovine serum albumin (BSA) in a solution of 0.3% Triton X-100 in PBS (PBS-Tx), for 1 hour at room temperature. After three rinses in PBS, sections were gently shaken overnight at room temperature in a solution of mouse monoclonal SMI-32 antibody (1:5000, Covance Research Products, Cat. no. SMI-32R-500, RRID:AB_509998) in 2% BSA diluted in 0.3% PBS-Tx. Sections were then washed three times in PBS, incubated in biotinylated secondary horse antimouse antibody (1:200, Vector Laboratories, Burlingame, CA) for 2 hours, at room temperature, washed again (3 × 10 minutes in PBS) and incubated for 1 hour in the Vectastain ABC System (1:500 Vector Laboratories) at room temperature. Immunoreactivity was revealed with 0.05% 3,3′-diaminobenzidine (DAB) and 0.1% nickel ammonium sulfate. Sections were then mounted on bi-gelatinized slides, dehydrated in increasing alcohol concentrations (75–90–100–100%, 1 minutes each), defatted in xylene (2 × 3 minutes), and coverslipped with DPX.

Data analysis

Photomicrographs of cortical sections were obtained using a Zeiss Axioplan-2 microscope equipped with a color digital camera (1,600 × 1200, 3/4″chip, 36bit, MicroBrightField, Colchester, VT, MBF) and a motorized stage (Mac5000 LUDL) controlled by Neurolucida software (MBF Biosciences; RRID:nif-0000-10294) running on a Dell workstation. Images from entire histological slides were produced with the aid of Virtual Tissue 2D

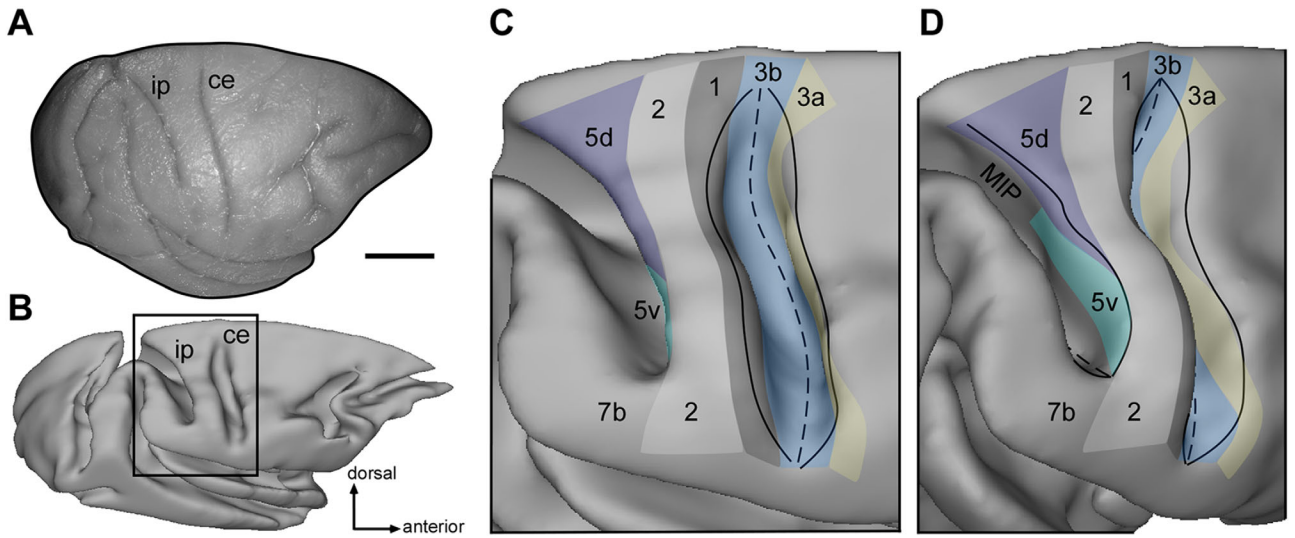

Figure 1. Sulcal pattern and architectonic subdivisions of cebus monkey cortex. **A:** Photograph of the right hemisphere in oblique view. **B:** 3D reconstruction at the level of cortical layer 4 of the hemisphere shown in A. Reconstruction at this laminar level allows an inside view of the cortex deepened into the sulci. The black rectangle delimitates the region of interest containing the parietal cortex, enlarged in C,D. **C:** Different colors depict areal subdivisions of the somatosensory cortex based on the architectonic data obtained for this case. The continuous line represents the contours of an opened central sulcus (ce). The dashed line represents the fundus of ce. Note that area 3a and part of 3b are located in the anterior bank of ce. **D:** In order to better expose cortical areas inside the anterior bank of the intraparietal sulcus (ip), the 3D reconstruction shown in C was rotated to provide a more caudal and lateral view. ce = central sulcus, ip = intraparietal sulcus, MIP = medial intraparietal area. Scale bar = 1 cm in A (applies to B). [Color figure can be viewed in the online issue, which is available at wileyonlinelibrary.com.]

module. With this software running in the Neurolucida system, a series of optical images of adjacent parts of a same section was systematically acquired, using a 5× (Zeiss Plan-Neofluoar) objective, and then unified in a single image of the whole section. Before image acquirement, color balance was adjusted to reduce background noise. Additional brightness and contrast correction was performed in the acquired image as a whole.

Borders between areas were established only after agreement between at least three independent investigators. The criteria used to differentiate cortical areas and establish area borders in sections immunoreacted for SMI-32 included size, density, and laminar distribution of immunoreactive cell bodies. Additional criteria included the extension and thickness of reactive apical dendrites, and intensity of neuropil reactivity in different cortical layers. In myelin-stained sections, stained axons were analyzed in relation to density, orientation (vertical or horizontal organization), and laminar distribution. In Nissl-stained sections, differences between cortical areas were established depending on differences in cell body size, density, and laminar distribution. Differences in laminar thickness between cortical areas were another criteria used to delimitate cortical areas.

3D reconstruction of anatomical borders

In one case, we performed a 3D reconstruction of the cortical surface using CARET software (Van Essen et al., 2001) to illustrate the spatial organization of somatosensory areas and the IPS in cebus monkey. Contours of sections immunoreacted for SMI-32 containing the limits of cortical layer 4 were drawn in Neurolucida. Borders between different cortical areas were marked in these drawings. All contours (with marked borders) were then combined in the Neurolucida software in order to produce a single *xml* file. This file was then edited in two steps. First, the file was manually split into two other files: one containing the *x,y,z* coordinates of the contours, and another file containing the *x,y,z* coordinates of the markers used to delimitate cortical area borders. In the second step, using a homemade program, these two separate files were converted to formats that could be read by CARET software (*.contour* and *.countour_cells*). Finally, after edition, these two files were imported to CARET and used to obtain the 3D reconstruction of the parietal cortex and its architectonic borders.

RESULTS

We used different staining methods in alternate sections of the same hemisphere to characterize

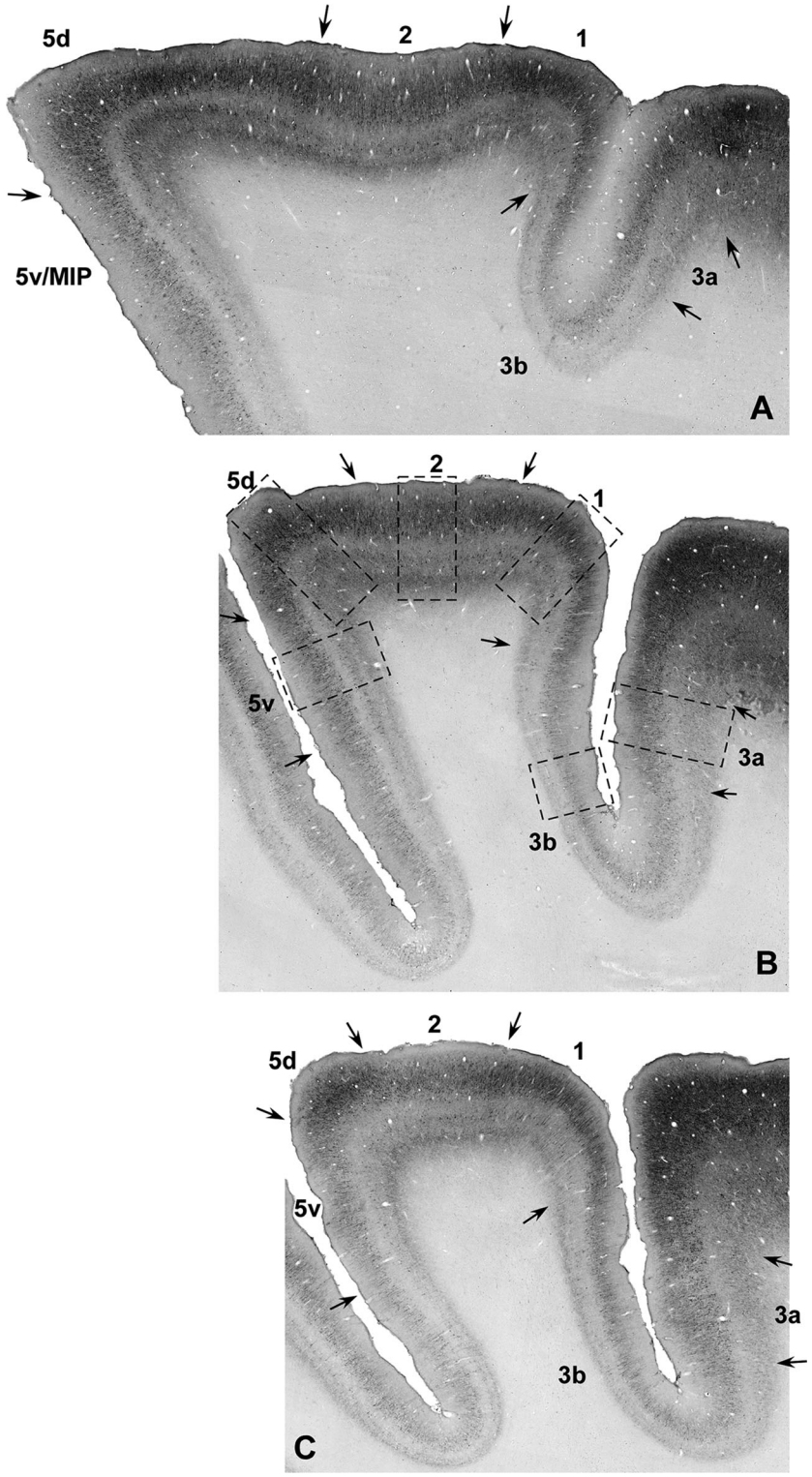

Figure 2. Low-magnification photomicrographs of parasagittal sections from the anterior portion of the parietal cortex immunoreacted for SMI-32 (case 13-01). **A–E:** Histological sections running from medial to lateral, with A being the medialmost section. Cortical boundaries are indicated by arrows above and/or below the cortical sheet. The portion of the parietal cortex illustrated in A–E is framed by gray boxes in schematic drawings of each section shown in **F**. In these micrographs, the posterior bank of the intraparietal sulcus was removed and only the anterior bank is apparent. The approximate level of each section is indicated by lines in the schematic drawing of a dorsal view of the right hemisphere illustrated in F (top right). Black dashed rectangles in B correspond to cortical regions enlarged in Figs. 4B1, 4B2, 7B1, 7B2, 8B1, 8B2. In each micrograph, dorsal is up and anterior is to the right, as shown by the indicative arrows in the inferior left corner of F. Scale bar = 2 mm in E (applies to A–E).

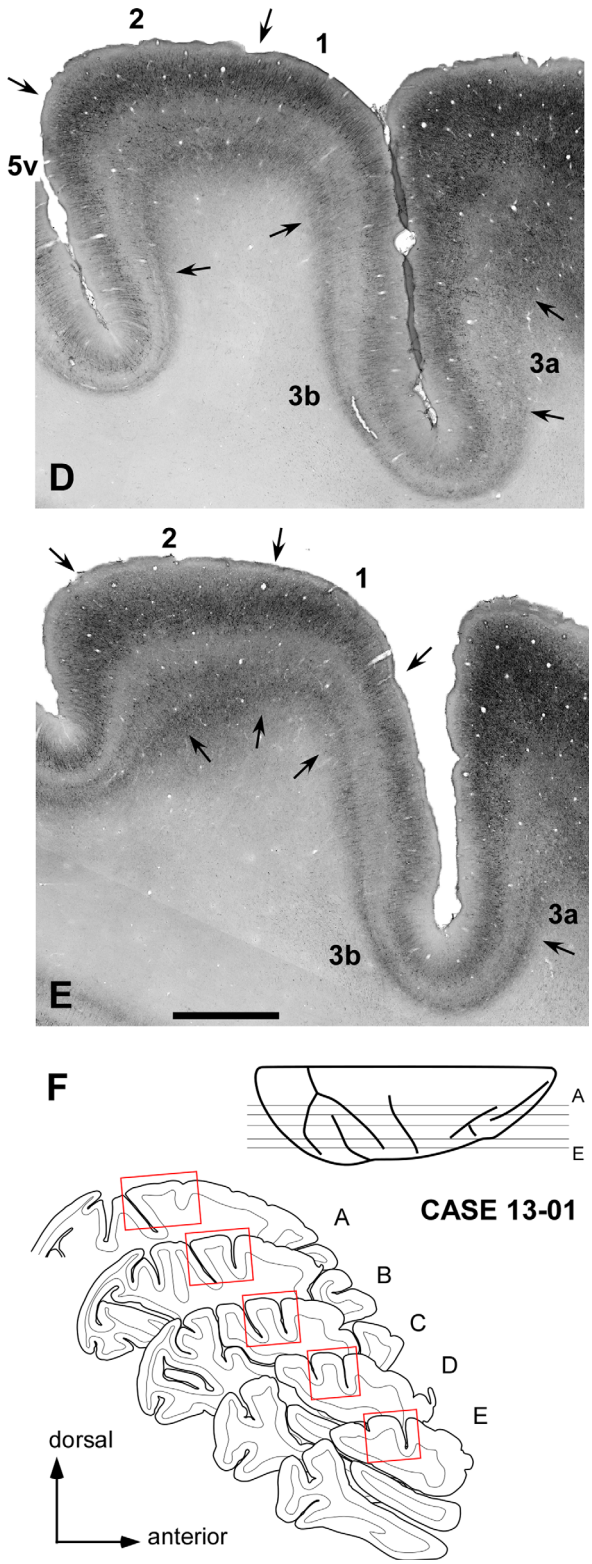

Figure 2. (continued) [Color figure can be viewed in the online issue, which is available at wileyonlinelibrary.com.]

architectonic subdivisions of cebus monkey somatosensory cortex. Seven different cortical areas were identified between the anterior bank of the central sulcus (CS) and the anterior bank of the intraparietal sulcus (IPS, Fig. 1). These areas included areas 3a, 3b, 1, 2, dorsal area 5 (5d), ventral area 5 (5v), and the medial intraparietal area (MIP). We adopted the same nomenclature applied to other primates (e.g., Nelson et al., 1980; Pandya and Seltzer, 1982; Pons et al., 1985; Lewis et al., 1999; Lewis and Van Essen, 2000; Krubitzer et al., 2004; Padberg et al., 2007) because the cortical areas identified here exhibited similar location and architectonic features as those previously described in macaque monkeys.

Although some staining variations were observed between cases (see "Technical considerations" in Discussion), the arrangement of cortical areas was highly consistent between all eight animals analyzed in this study. As for the myelin stain, we observed a relative lack of impregnated fibers in layers 1 and 2 that were refractory to our staining procedure. Figure 1 illustrates the topographical distribution of the cortical areas described in this study. Area 3a was located in the anterior bank of the CS. Close to the lateral and medial tips of the CS, area 3a extends to the exposed cortical surface, anterior to area 3b. Area 3b extends from the anterior to the posterior bank of the CS. Caudal to area 3b, area 1 occupies part of the posterior bank and the entire mediolateral extension of the posterior margin of the CS. Area 2 corresponds to a strip of neocortex located in the middle of the postcentral gyrus running in a medial to lateral orientation somewhat parallel to the CS. Area 5d is located posterior to area 2, occupying the most posterior part of the postcentral gyrus, but it is predominantly located in the anterior margin of the IPS. Area 5v is found ventrolaterally to area 5d and ventroposteriorly to area 2 in the anterior bank of the IPS, extending laterally up to the tip of the sulcus.

Architectonic characterization of somatosensory areas

Area 3a

In sections immunoreacted for SMI-32, area 3a was identified by a well-stained layer 3 (Figs. 2, 3), characterized by moderate density of middle-sized labeled pyramidal cell bodies with thin apical dendrites (Fig. 4B1). Infragranular layers were differentiated by a generally weak immunoreactivity consisting of sparse mid- to large-size cell bodies in layer 5 and weak neuropil staining in layer 6 (Figs. 3, 4B1). Compared to the immediately neighboring areas 3b and M1, area 3a presented stronger immunoreactivity than area 3b, especially in layer 3, and weaker immunoreactivity than area M1 (Fig. 2), particularly in layer 5, which clearly showed lower density of labeled cells (Fig. 3).

Area 3a was slightly more myelinated than both areas 3b and M1 (Figs. 5, 6). A roughly bilaminar appearance could be identified due to some heterogeneity in layer 5. The superior portion of layer 5 exhibited intense myelination, whereas the inferior portion was slightly less myelinated. Different from area 3b, infragranular layers of area 3a presented thick myelinated fibers oriented towards the pial surface, especially in layer 6 (compare Fig. 4C1 with C2). However, these vertically oriented fibers were not as easily visualized as in area 1 (see below) due to a high density of vertically and nonvertically oriented (matted) fibers in the same region. Layer 4 presented relatively low myelination, consisting of sparse fibers with no particular orientation (Fig. 4C1).

In Nissl stain, area 3a exhibited a poorly developed layer 4, and a distinctive homogenous appearance, which was the best criteria to differentiate it from the neighboring areas 3b and M1, especially at low magnification (Fig. 5C). Area 3a displayed well-developed layers 3 and 5 populated with dense and sparse mid-size cell bodies, respectively (Fig. 4A1). Layer 6 was thick, but did not present a clear border with layer 5. In accordance with the vertically oriented fibers revealed by the myelin staining, in Nissl, infragranular layers presented vertical stacks of neuronal cell bodies, indicative of minicolumnar organization. This can be used as a good criterion to identify the inferior limit of layer 4.

Area 3b

As expected, area 3b presented a well-defined layer 4 with densely packed small- to medium-sized granular cell bodies. Although a portion of area 3b could be found in the anterior bank of the CS, most of area 3b was located in the fundus and posterior bank of the CS, occupying a strip of cortex running along the entire mediolateral extension of the sulcus (Fig. 1C). Due to the curvature of the cortical sheet, the portion of area 3b located in the fundus of the sulcus exhibited wider supragranular layers and thinner granular and infragranular layers than the portion located in the posterior bank of the sulcus. Because the largest extent of area 3b was found in the posterior bank of the CS, the architectonic description provided here was based on this portion of area 3b.

Area 3b showed low immunoreactivity for SMI-32, especially when compared with neighboring area 3a (Figs. 2, 3). Sparse small-sized cell bodies with long apical dendrites were stained in layer 3 (Fig. 4B2). Layer 6

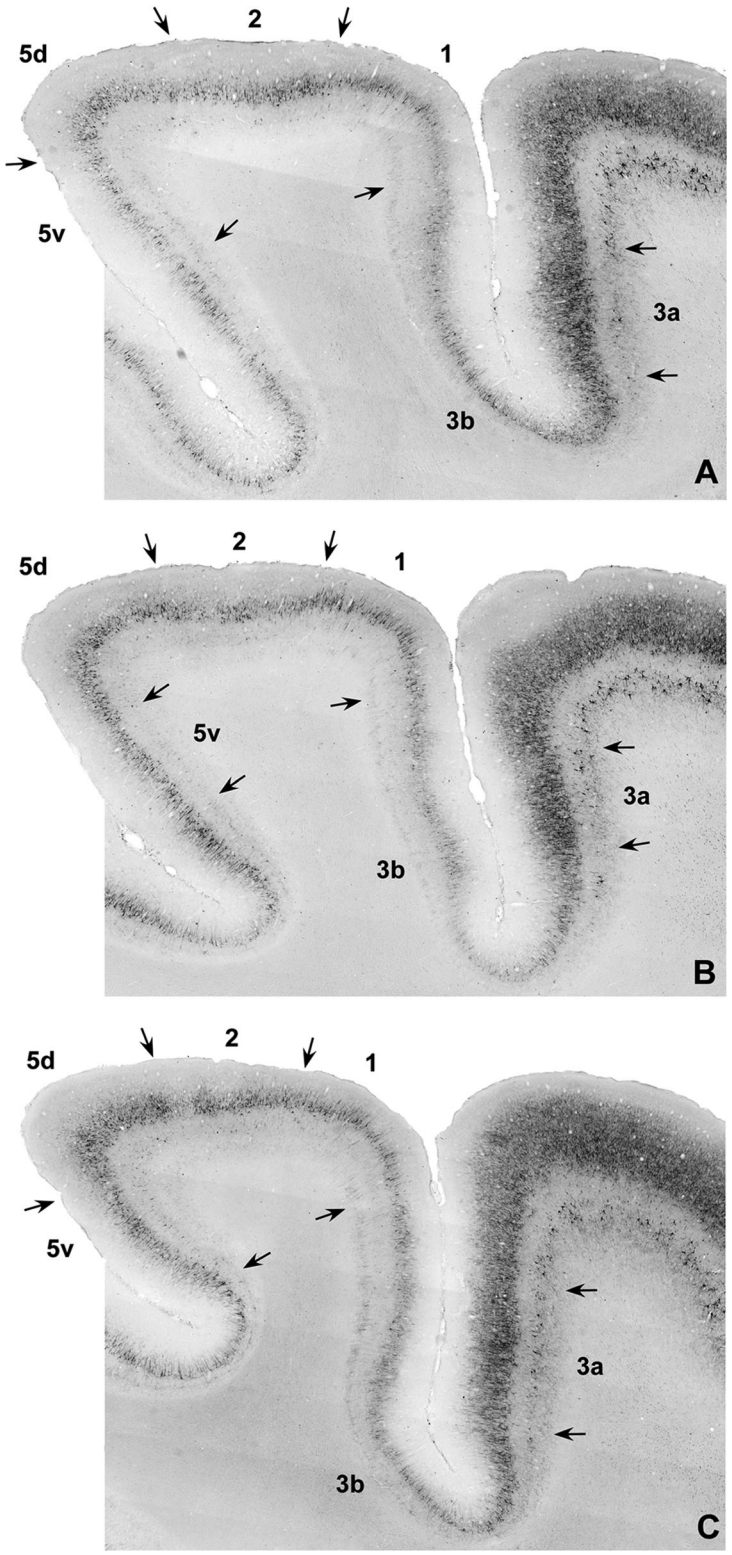

Figure 3. Low-magnification photomicrographs of parasagittal sections from the anterior portion of the parietal cortex immunoreacted for SMI-32 (case V2-02). **A–E:** Histological sections running from medial to lateral, with A being the medialmost section. Cortical boundaries are indicated by arrows above and/or below the cortical sheet. The portion of the parietal cortex illustrated in A–E is framed by red boxes in schematic drawings of each section shown in **F**. In these micrographs the posterior bank of the intraparietal sulcus was removed and only the anterior bank is apparent. The approximate level of each section is indicated by lines in the schematic drawing of a dorsal view of the right hemisphere illustrated in F (top left). In each micrograph, dorsal is up and anterior is to the right, as shown by the indicative arrows in the inferior right corner of F. Scale bar = 2 mm in E (applies to A–E). [Color figure can be viewed in the online issue, which is available at wileyonlinelibrary.com.]

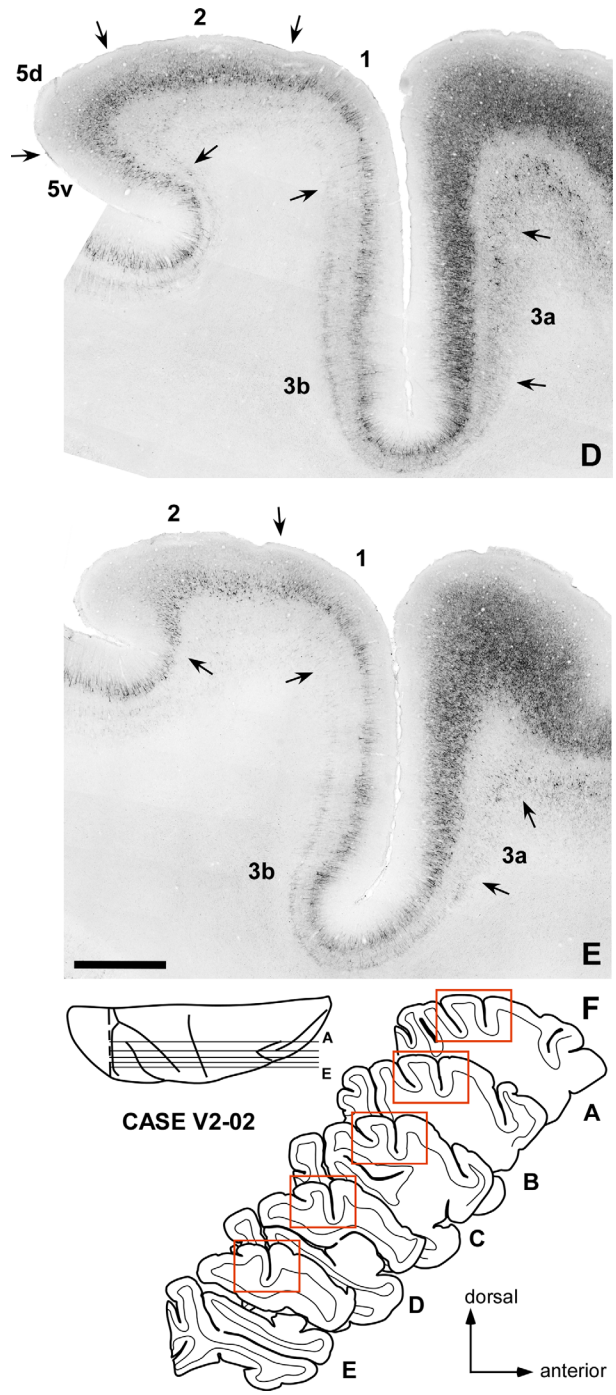

Figure 3. (continued)

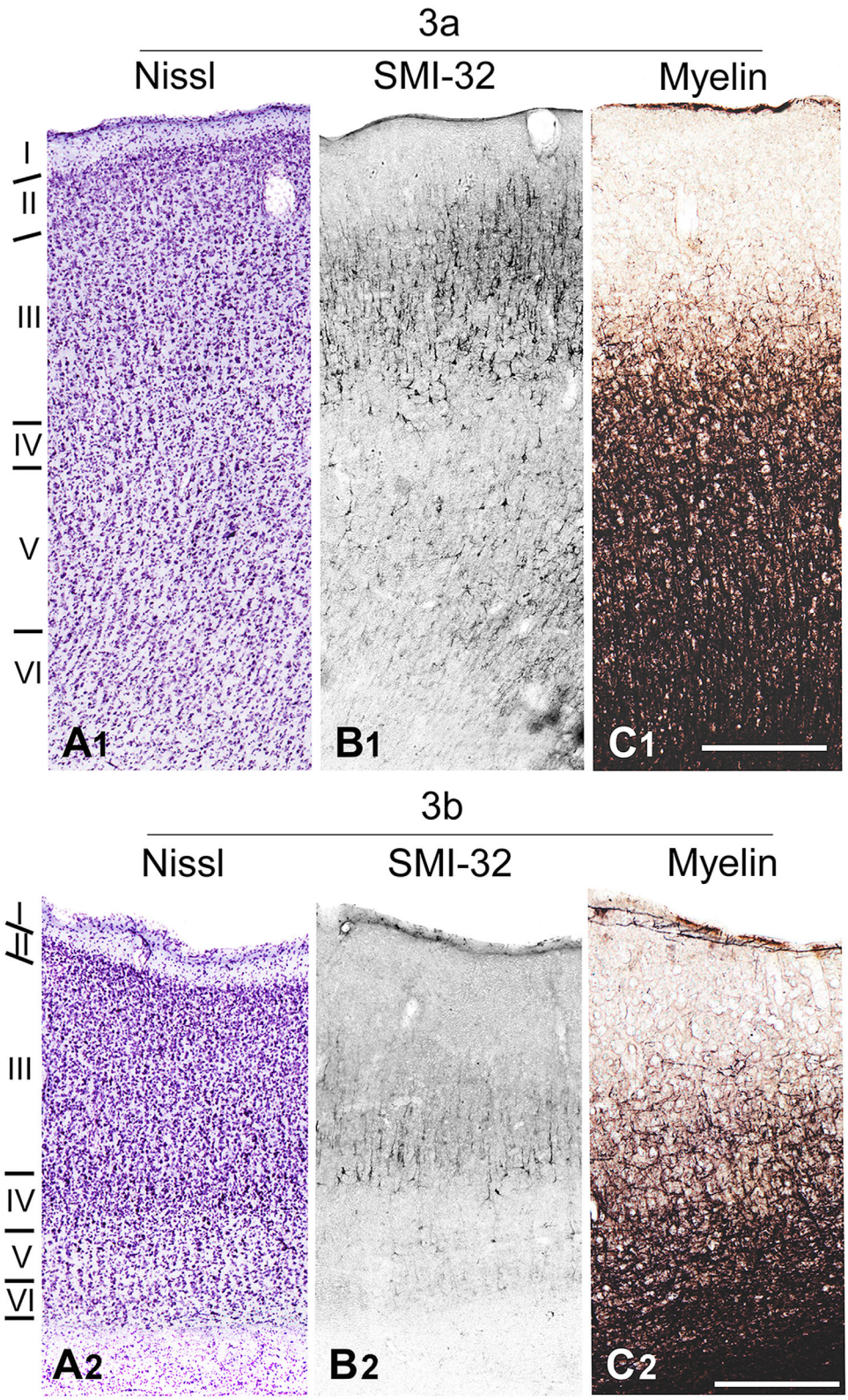

Figure 4. Photomicrographs at high magnification showing the architecture of areas 3a (top) and 3b (bottom) revealed by Nissl staining **(A)**, SMI-32 immunoreactivity **(B)**, and myelin staining **(C)**. Photomicrographs showing SMI-32 immunoreactivity were all taken from the section shown in Fig. 2B (black dashed boxes). Nissl-stained sections correspond to adjacent sections of the same hemisphere. Photomicrographs of myelin stain correspond to white dashed rectangles depicted in Fig. 5B. Scale bars = 500 μm in C1 and C2 applies to all plates from areas 3a and 3b, respectively. [Color figure can be viewed in the online issue, which is available at wileyonlinelibrary.com.]

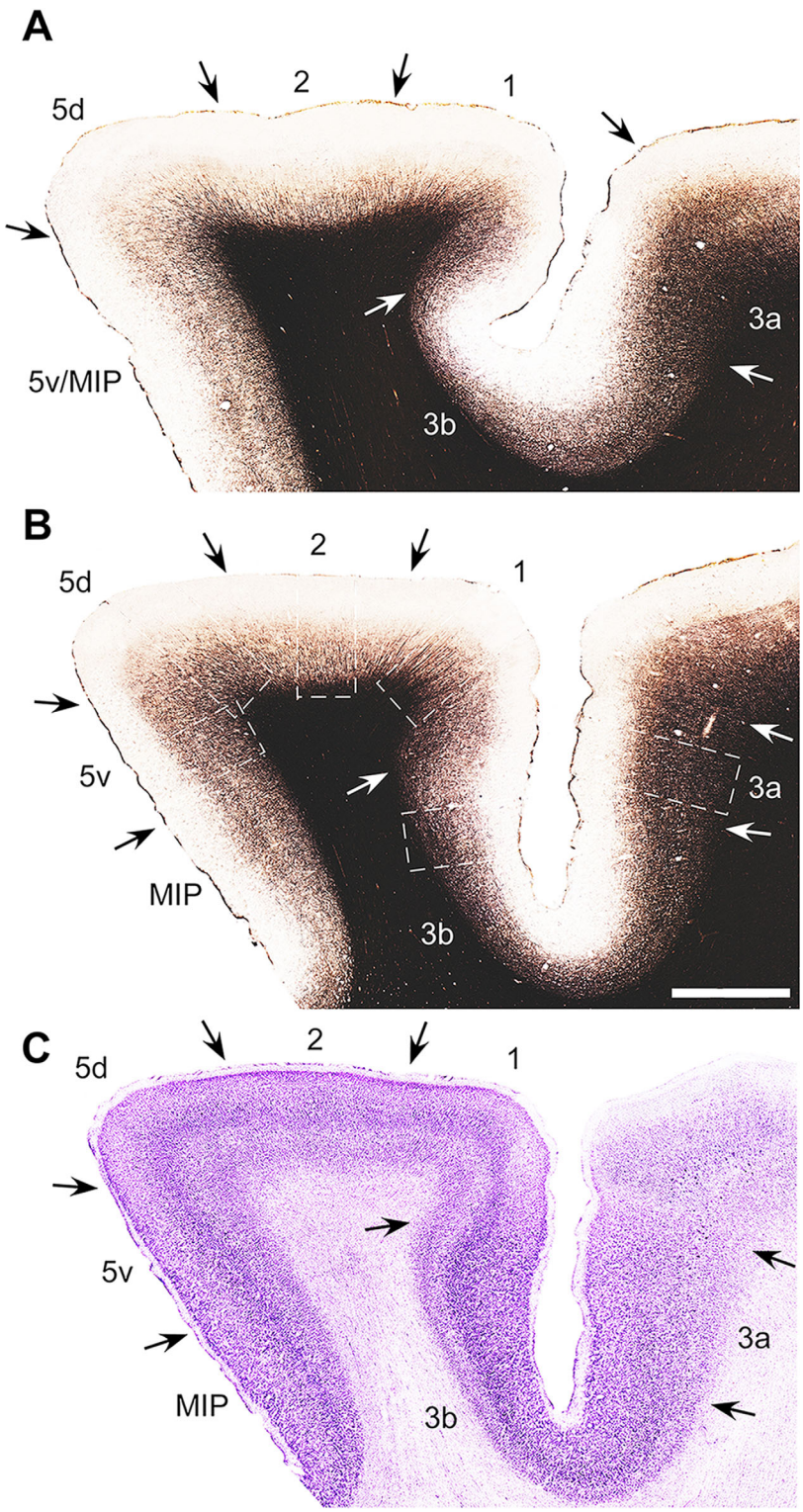

Figure 5. Low-magnification photomicrographs of parasagittal sections from anterior portions of the parietal cortex stained for myelin and Nissl (case 08-01). Cortical boundaries are indicated by arrows above and/or below the cortical sheet. **A,B,D,E:** Myelin-stained sections, with A being more medial. **C:** A cresyl violet-stained section adjacent (lateral) to B. The portion of the parietal cortex illustrated in A,B,D,E is framed by brown boxes in schematic drawings of each section shown in **F**. The anterior bank of intraparietal sulcus and the anterior and posterior banks of the central sulcus are shown in all plates. Approximate level of the sections is indicated by lines on the schematic drawing of a dorsal view of the right hemisphere shown in F (top right). White dashed rectangles in B correspond to cortical regions enlarged in Figs. 4C1, 4C2, 7C1, 7C2, 8C1, 8C2. In each micrograph dorsal is up and anterior is to the right, as shown by the indicative arrows in the inferior left corner of E. Scale bars = 2 mm in B,E (applies to all). [Color figure can be viewed in the online issue, which is available at wileyonlinelibrary.com.]

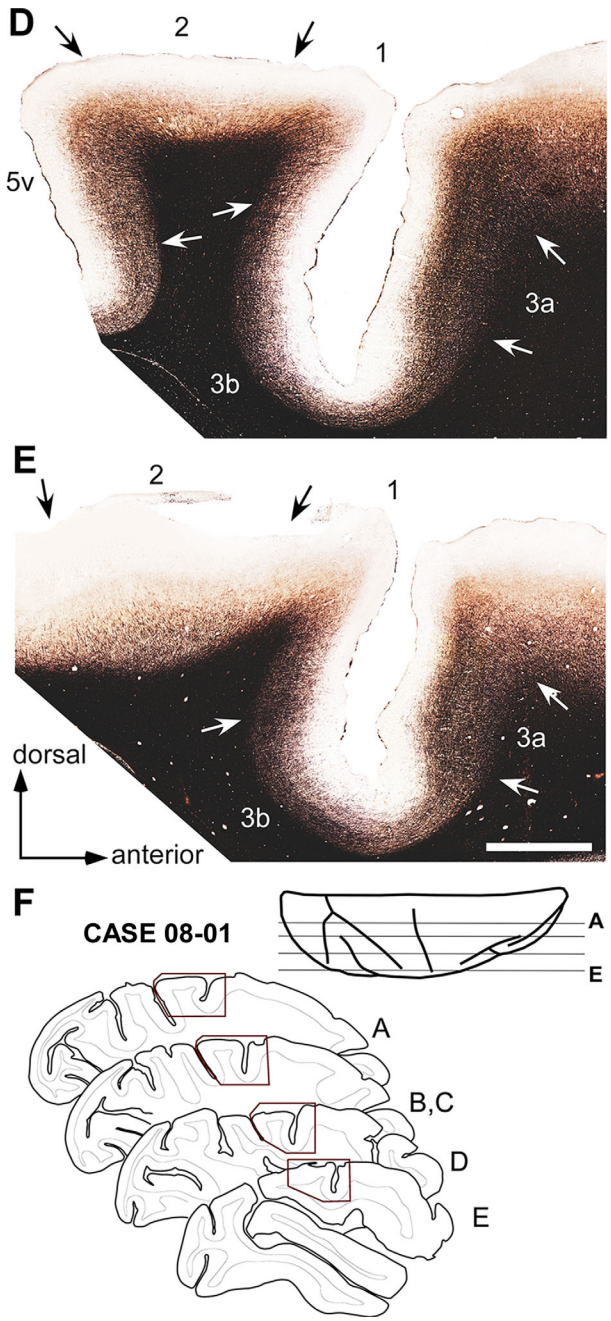

Figure 5. (continued) [Color figure can be viewed in the online issue, which is available at wileyonlinelibrary.com.]

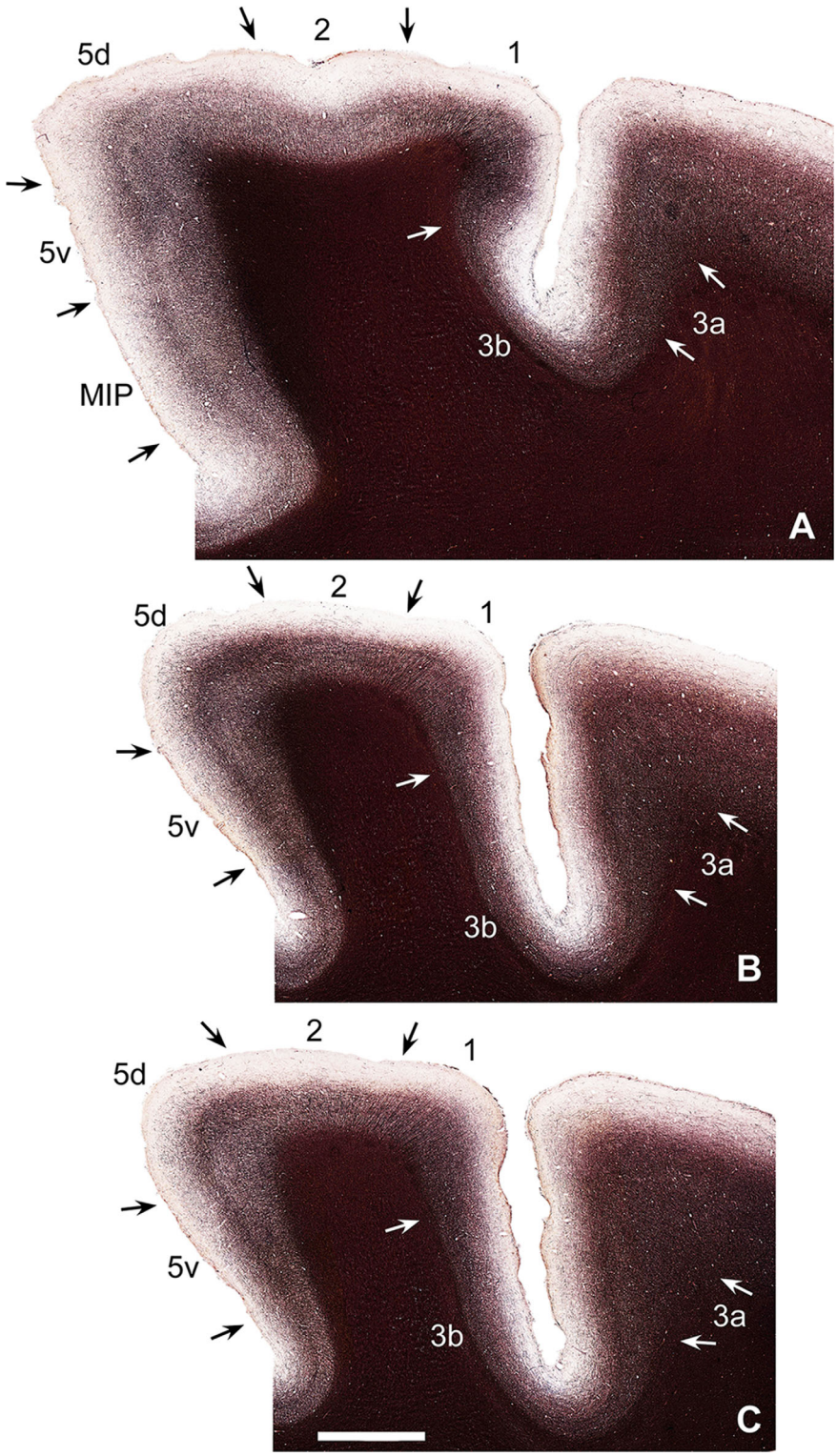

Figure 6. Low-magnification photomicrographs of parasagittal sections from anterior portions of the parietal cortex stained for myelin (case CB-78). Cortical boundaries are indicated by arrows above and/or below the cortical sheet. **A–E:** Histological sections running from medial to lateral, with A being the medialmost section. The portion of the parietal cortex illustrated in A–E is framed by red boxes in schematic drawings of each section shown in **F**. The anterior bank of intraparietal sulcus and the anterior and posterior banks of the central sulcus are shown in all plates. Approximate level of the sections is indicated by lines on the schematic drawing of a dorsal view of the right hemisphere shown in F (top right). In each micrograph (A–E) dorsal is up and anterior is to the right, as shown by the indicative arrows in the inferior left corner of F. Scale bars = 2 mm in C,D (applies to all). [Color figure can be viewed in the online issue, which is available at wileyonlinelibrary.com.]

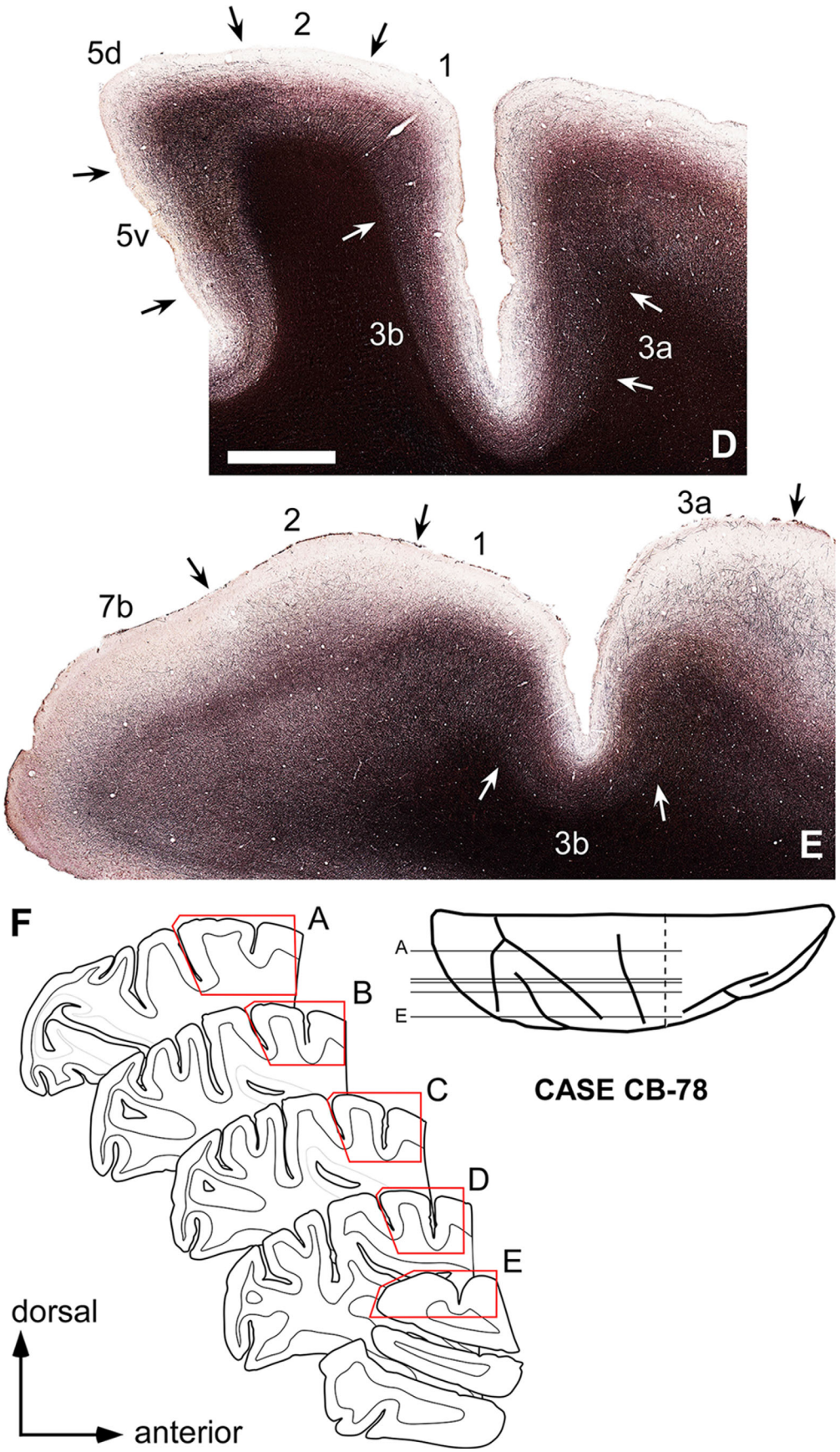

Figure 6. (continued) [Color figure can be viewed in the online issue, which is available at wileyonlinelibrary.com.]

presented a very weak, sometimes absent, diffuse neuropil labeling. Area 3b exhibited a very poorly labeled layer 5 (Figs. 2, 3), with few small-sized cell bodies and almost no neuropil labeling (Fig. 4B2).

Infragranular layers were intensely myelinated, with predominance of a dense horizontal fiber net, especially in layer 6 (Figs. 4C2, 5, 6). Layer 4 also presented horizontal fibers, but less densely stained than in layer 6, resulting in a bilaminar appearance. Area 3b typically exhibited labeled fibers in layer 1 (Fig. 4C2). These fibers were sparse, thick, and more visible at the medial portion of the hemisphere.

Nissl stain revealed that layers 4 and 6 were well developed, consisting of densely packed small- and mid-size cell bodies (Figs. 4A2, 5C), similar to what was previously reported in macaque monkeys (Nelson et al., 1980; Pons et al., 1985). Contrasting with neighboring areas 1 and 3a, and in accordance with the SMI-32 immunohistochemistry, area 3b presented a poorly developed layer 5 (compare Fig. 4A2 with A1). Layer 3, on the other hand, was much thicker in area 3b than in most of the other cortical areas of the anterior parietal cortex.

Area 1

Area 1 could be clearly distinguished from neighboring areas 3b and 2 due to the moderate to intense SMI-32 immunoreactivity found in layer 3 with a peculiar vertically striated appearance (Figs. 2, 3 and 7B1), similar to what was previously reported in the macaque monkey (Lewis et al., 1999). Layer 3 consisted of dense mid-size cell bodies with elongated apical dendrites extending up to layer 2 (Fig. 7B1). The distinctive vertically striped appearance of area 1 was due to labeled axons and dendritic neuropil in layers 2 and 6 that exhibited a radial and elongated aspect. Layer 5 presented a low to moderate density of labeled cell bodies and some neuropil labeling in layer 6 (Fig. 7B1).

Area 1 presented a very distinctive myeloarchitecture characterized by intense myelination, distinctively more intense than that of area 2, and also by the presence of long and thick vertical myelinated fibers in infragranular layers, extending through layers 6 and 5, up to layer 4 (Fig. 7C1). Different from area 3a (Fig. 4C1), in which the staining was very intense, individual vertical fibers of area 1 could be very clearly identified. This anatomical feature, as in SMI-32 immunohistochemistry, gave area 1 a particular palisade-like appearance.

In accordance with SMI-32 immunohistochemistry and myelin stain, a clear palisade-like appearance was also observed in Nissl-stained sections (Fig. 7A1). At low magnification, layers 4 and 6 were well delimited, more conspicuous than the corresponding layers in area 2, but not as evident as in area 3b (Fig. 4A2). Another distinctive feature of area 1 was the apparent subdivision of layer 3 (Fig. 7A1). The upper part of the layer, sublayer 3a, was composed of dense small-sized cell bodies. Sublayer 3b consisted of mid- and large-sized cell bodies, more sparsely packed than in sublayer 3a.

Area 2

In the medial portion of area 2, a lighter SMI-32 immunoreactivity in layer 3 provided a reliable criterion to identify the border with areas 5d and 1 (Figs. 2A–C, 3A–C). The lower part of layer 3 (sublayer 3b, see below) presented a moderate density of immunostained mid-size pyramidal cell bodies with short apical dendrites (Fig. 7B2). Due to low immunoreactivity of the upper part of layer 3 (sublayer 3a), the supragranular band of SMI-32 labeling in area 2 appeared thinner than in areas 1 and 5d, especially at low magnification (Figs. 2, 3). In infragranular layers of the medial portion of area 2 (Fig. 2A–C) SMI-32 immunoreactivity was less intense than in area 5d but looked similar to that of area 1, with a moderate density of stained pyramidal cell bodies and axons in layer 5, and moderate to intense diffuse neuropil staining in layer 6 (Fig. 7B2). However, a different staining pattern was found in infragranular layers at more lateral portions of area 2 (Fig. 2D–F). Progressing from medial to lateral, a slight increase in the density of mid-size cell bodies in layer 5 and neuropil labeling in layer 6 was observed (compare Fig. 2A,B with D and E,F). Thus, in more lateral portions of the parietal cortex, area 2 could be distinguished from neighboring areas 1, 5v, and 7 by the more intense immunoreactivity found in infragranular layers, in addition to differences in the staining pattern of layer 3.

Area 2 was moderately myelinated, contrasting with the highly myelinated neighbors, areas 5d, 5v, and 1 (Figs. 5, 6). Despite this difference, the general myeloarchitecture of area 2 was similar to the one of area 5d (compare Figs. 7C2 with 8C2). Layer 4 presented low myelination (Fig. 7C2). In infragranular layers, a moderate density of thick and short vertically oriented fibers could be observed (Fig. 7C2), providing a columnar-like organization to these cortical layers, in the same orientation of the cellular columns observed in Nissl stain (Fig. 7A2).

At low magnification, area 2 presented a more homogeneous cytoarchitecture than neighboring areas (Fig. 5C). Although the rostral and caudal borders of area 2 were very difficult to identify in Nissl stain, the most reliable criteria to delimit this cortical area were the wider and less compact layers 4 and 6 (Fig. 7A2) and, in more lateral portions, a thicker layer 3 (Fig. 5C). Layer 3 of area 2 was subdivided into 3a and 3b (Fig.

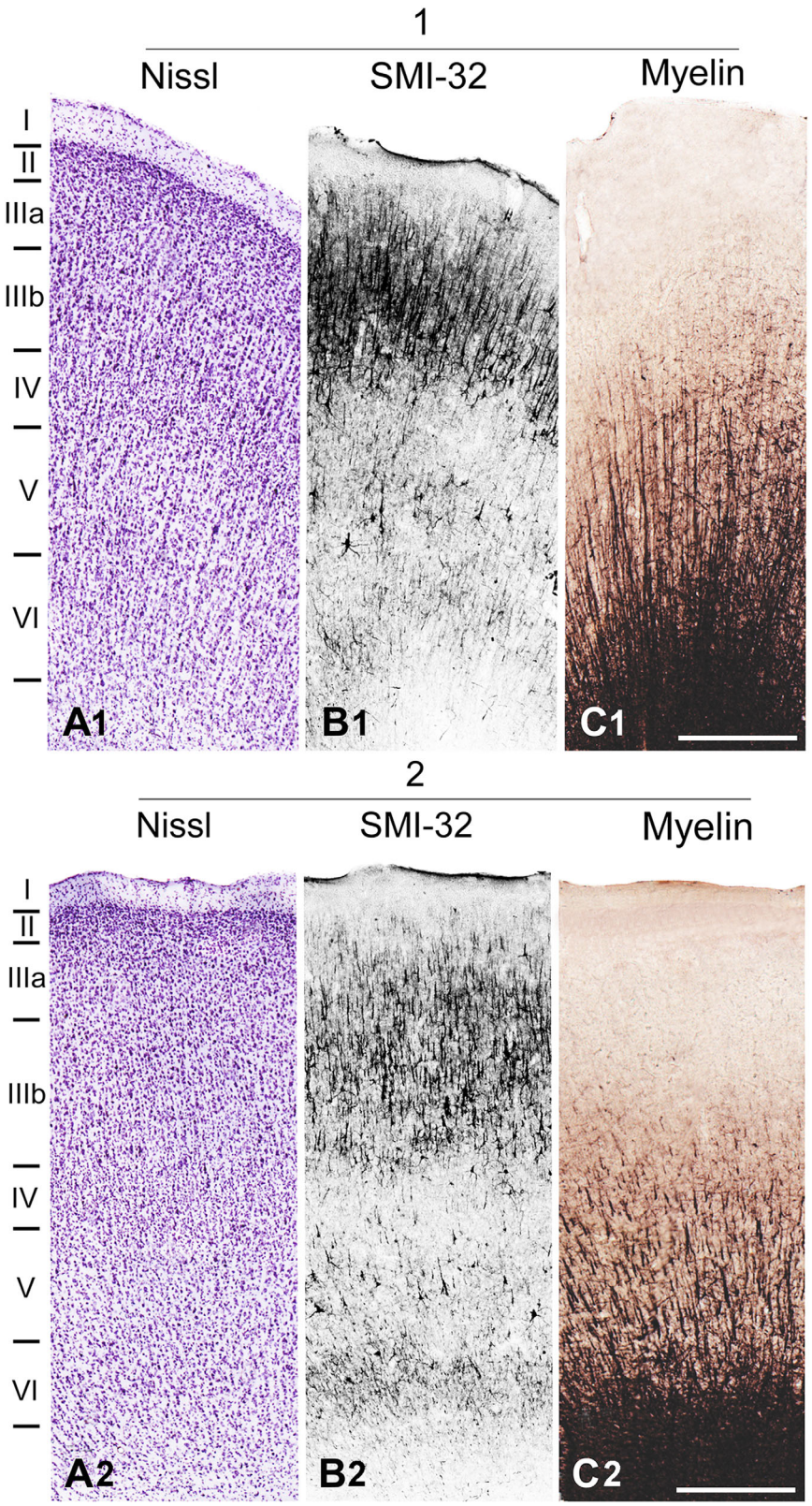

Figure 7. Photomicrographs at high magnification showing the architecture of areas 1 (top) and 2 (bottom) revealed by Nissl staining **(A)**, SMI-32 immunoreactivity **(B)** and myelin staining **(C)**. Photomicrographs showing SMI-32 immunoreactivity were all taken from the section shown in Fig. 2B (black dashed boxes). Nissl-stained sections correspond to adjacent sections of the same hemisphere. Photomicrographs of myelin stain correspond to white dashed rectangles depicted in Fig. 5B. Scale bars = 500 μm in C1 and C2 applies to all plates from areas 1 and 2, respectively. [Color figure can be viewed in the online issue, which is available at wileyonlinelibrary.com.]

7A2), but the delimitation of the sublayers was not as clear as in area 1. Layers 3b, 4, and 6 presented a clear columnar organization (Fig. 7A2).

Area 5

Similar to the parietal parcellation described in the macaque monkey (Lewis and Van Essen, 2000), area 5 in the cebus monkey was subdivided in two anatomically different sectors, areas 5-dorsal (5d) and 5-ventral (5v) (Fig. 1). Architectural differences between 5d and 5v were observed in all histological preparations. The best criteria to distinguish between these areas were differences in myeloarchitecture, followed by differences in SMI-32 immunoreactivity. Interestingly, area 5d exhibited more similarities with area 2 than with area 5v.

Area 5d

In sections immunoreacted for SMI-32, area 5d was characterized by moderate to intense immunoreactivity, with higher density of stained cells than neighboring areas 5v and 2 (Figs. 2A–D, 3A–C). The architecture of layer 3, however, was similar to area 2, consisting of mid-size cell bodies and short apical dendrites (compare Figs. 8B2 and 7B2). Area 5d exhibited a very distinct immunoreactivity in infragranular layers. Layer 5 was moderately to densely populated by mid- and large-sized cell bodies and intense neuropil labeling, especially in the most medial portion of the area. In layer 6 a moderate to intense neuropil labeling could be observed (Fig. 8B2).

Area 5d was intensely myelinated, especially when compared, at low magnification, with the neighboring area 2 (Figs. 5A,B, 6A–D). At higher magnification, however, except for a higher density of myelinated fibers, the myeloarchitecture of area 5d was similar to that of area 2 (Figs. 8C2 and 7C2, respectively). Infragranular layers presented a dense net of short and thick vertical fibers. They were also present in layer 4, but in a much lower density. Compared with the neighboring area 5v, area 5d exhibited a very different myeloarchitectonic pattern (see below).

Similar to areas 5v and 1, area 5d also exhibited a very clear lamination in Nissl-stained sections (Figs. 5C, 8A2). Layer 4 was more compact and discernible than in area 2. As in area 2, layer 3 of area 5d was subdivided into 3a and 3b, but not as clearly as in area 1. Infragranular layers were thicker than those of the cortical areas of the anterior parietal cortex. This difference was observed in other stains. This was probably due to the distortion provoked by the cortical curvature of the margin of the IPS, where area 5d was located. However, comparing the infragranular layers of area 5d with those of other areas that are likewise located on the margin of a sulcus, like area 1, one could presume that layers 5 and 6 of area 5d were actually well developed.

Area 5v

Area 5v presented a low to moderate SMI immunoreactivity, weaker than that in area 5d (Figs. 2, 3). Layer 3 exhibited low to moderate density of stained cell bodies with long apical dendrites (Fig. 8B1). SMI-32 staining differences in layer 3 could be used as a reliable criterion to distinguish between area 5v, 5d and 2 (Figs. 2, 3). Compared with area 5d, layer 3 of area 5v was less reactive. Intensity of immunoreactivity in layer 3 was similar to the one in area 2, but the layer thickness and the pattern of axon labeling were different. Layer 3 of area 5v was thinner and presented more elongated axons, whereas, in area 2, labeled axons were shorter. Another distinctive feature of area 5v was the staining pattern of infragranular layers. They presented weaker immunoreactivity than that of infragranular layers of areas 5d and 2 (Fig. 2). Layer 5 exhibited low density of reactive cell bodies (Fig. 8B1). Layer 6 presented weak to moderate diffuse neuropil labeling (Fig. 8B1), sometimes similar to what is found in area 2.

Among all analyzed areas, area 5v was the only one in which bands of Baillarger could be clearly observed in myelin stain (Figs. 5B, 6A–D). At low magnification, this feature was the best criterion to differentiate this cortical area from the neighboring area 5d. As described before, area 5v exhibited a myeloarchitectonic pattern very distinct from area 5d (Figs. 5A,B, 8C1,C2). Layer 6 presented intense myelination, consisting of a net of thin horizontal fibers and long and thick vertical fibers, extending up to layer 5. In contrast to the pattern of neighboring areas, layer 4 showed rich myelination, with dense matted fibers (outer band of Baillarger, Fig. 8C1). Layer 5 displayed intermediate myelination (inner band of Baillarger), consisting predominantly of thin horizontal fibers.

Contrasting with area 5d, area 5v exhibited a poorly developed layer 5 in Nissl stain (Fig. 8A1). Layers 4 and 6 were well defined (Figs. 5C, 8A1). Layer 3 of area 5v was subdivided into 3a and 3b (Fig. 8A1), but the border between these sublayers was not as clear as in area 1. Similar to what was observed in myelin stain, infragranular layers showed a minicolumnar organization, characterized by stacks of cell bodies especially in layer 6, where vertical thick myelinated fibers were predominant (Fig. 8A1,C1). Those minicolumns could be observed in almost the entire area 5v, especially in layers 4, 5, and 6.

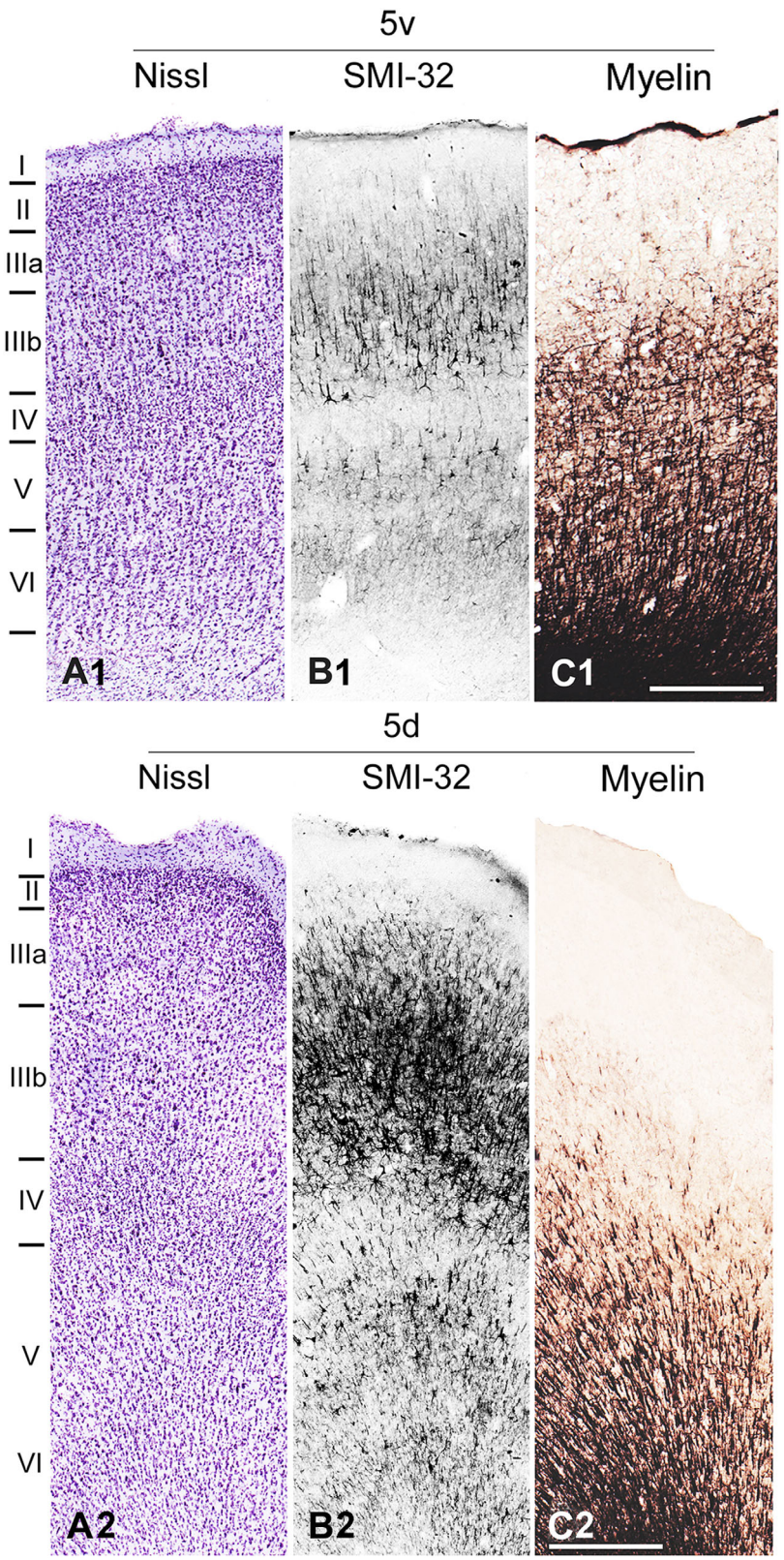

Figure 8. Photomicrographs at high magnification showing the architecture of areas 5v (top) and 5d (bottom) revealed by Nissl staining **(A)**, SMI-32 immunoreactivity **(B)** and myelin staining **(C)**. Photomicrographs showing SMI-32 immunoreactivity were all taken from the section shown in Fig. 2B (black dashed boxes). Nissl-stained sections correspond to adjacent sections of the same hemisphere. Photomicrographs of myelin stain correspond to white dashed rectangles depicted in Fig. 5B. Scale bars = 500 μm in C1 and C2 applies to all plates from areas 5v and 5d, respectively. [Color figure can be viewed in the online issue, which is available at wileyonlinelibrary.com.]

Caudal border of area 2

The caudal border of area 2 was inconspicuous in Nissl stain. In SMI-32 immunohistochemistry and myelin stain, the boundary of area 2 with areas 5v and, especially, with 5d, medial to the tip of IPS, could be clearly visualized (Figs. 2A–E, 3A–E, 5A,B,D, 6A–D). However, lateral to the IPS, the border of area 2 with area 7 (Fig. 1) was not as evident as the border with area 5 in any of the histological protocols used in this study, including SMI-32 immunohistochemistry and myelin stain (Figs. 5E, 6E). The most distinctive feature of area 2 in this region of the parietal cortex was that supragranular layers were thicker than in area 7 immediately caudal to it (see supragranular SMI-32 immunostaining in Fig. 9B). Therefore, to better locate and characterize the boundary between areas 2 and 7, somatosensory mappings were performed around and lateral to the tip of IPS. In anesthetized preparations, the physiological border between area 2 and area 7 should correspond to the transition from cortex responsive to somatosensory stimulation to a more caudal and unresponsive cortical region, respectively (Pons et al., 1985). As shown in Fig. 9, the functional border correlated well with the architectonic border (corresponding to the most caudal red dashed line in the schematic drawings of Fig. 9). However, some variability in the position of the caudal border of area 2 was observed when different cases were compared. One confounding factor was the occasional appearance of a few unresponsive sites in area 2 (Fig. 9C,D), and some somatosensory responses in neurons located in area 7 (Figs. 9C,E). This was not surprising, considering that somatosensory responses can be mapped in area 7b (i.e., PF and PFG) in awake animals (Rozzi et al., 2008). Thus, our somatosensory recordings in area 7 might be due to some variability in anesthetic levels during the mapping, and/or to individual differences in sensibility to anesthesia. Still, the functional border presented a good correlation with the anatomical border.

DISCUSSION

In a previous work we successfully used SMI-32 immunohistochemistry, myelin, and Nissl stains in alternate cortical sections to characterize the organization of the somatosensory and visual cortex of the rodent agouti (Dias et al., 2014). In the current study we adopted the same approach to the parietal cortex of the cebus monkey and we identified seven architectonically distinct areas located between the anterior bank of the CS and the anterior bank of the IPS. Besides the architectonic identification of areas 3a, 3b, 1, and 2, our data indicated that area 5 of Brodmann could be subdivided into three sectors: areas 5d, 5v, and MIP. The borders between the subdivisions of area 5, as well as the caudal and rostral borders of area 2, could be clearly identified in SMI-32-immunostained sections and myelin stain, but not in Nissl-stained sections.

Technical considerations

Some staining variability was observed in the different cases analyzed. For instance, in the material presented in Fig. 2 (case 13-01), the SMI-32 immunoreactivity was generally more intense than the case presented in Fig. 3 (case V2-02). We could clearly see infragranular labeling in case 13-01, while in case V2-02, because of the less intense background reactivity, architectonic features of supragranular layers were more easily identified. In some sections of case 13-01, a general dorsal-to-ventral staining gradient, not observed in case V2-02, was present. However, both cases revealed the same immunostaining pattern.

A similar variation was observed in the two myelin stains in the cases presented in Fig. 5 (case 08-01) and Fig. 6 (case CB-78). In case 08-01, we obtained a lighter myelin staining, especially in supragranular layers. This staining pattern allowed a better characterization of the fiber organization in granular and infragranular layers in this case. Considering all together, cases were complementary to each other. In none of our cases did we observe a bundle of impregnated fibers in layers 1 and 2, as described in humans by Budde and Annese (2013).

One important factor that could account for this kind of variation in staining was the previous exposure of the cortical surface under study to experimental procedures, such as electrophysiological recording and/or tracer injections performed for a related study (see Materials and Methods). This occurred in cases 13-01 and 08-01, but not in cases V2-02 and CB-78. However, it is important to note that the consistency of the staining pattern obtained in the different cases studied corroborates the reliability of our findings.

We also have to take into account that the plane of section modifies the apparent length of labeled axons and apical dendrites. It is expected that labeled axons and apical dendrites would display much smaller lengths in a section cut parallel to the cortical sheet. In the present study all myelin staining and SMI-32 immunohistochemistry were performed on parasagittal sections. Therefore, in medially located sections labeled axons and apical dendrites would appear longer than in more lateral sections that are located closer to the lateral cortical convexity. However, except for the lateralmost sections (e.g., Figs. 5E, 6E), these variations were not perceptible in the sections sampled for this study.

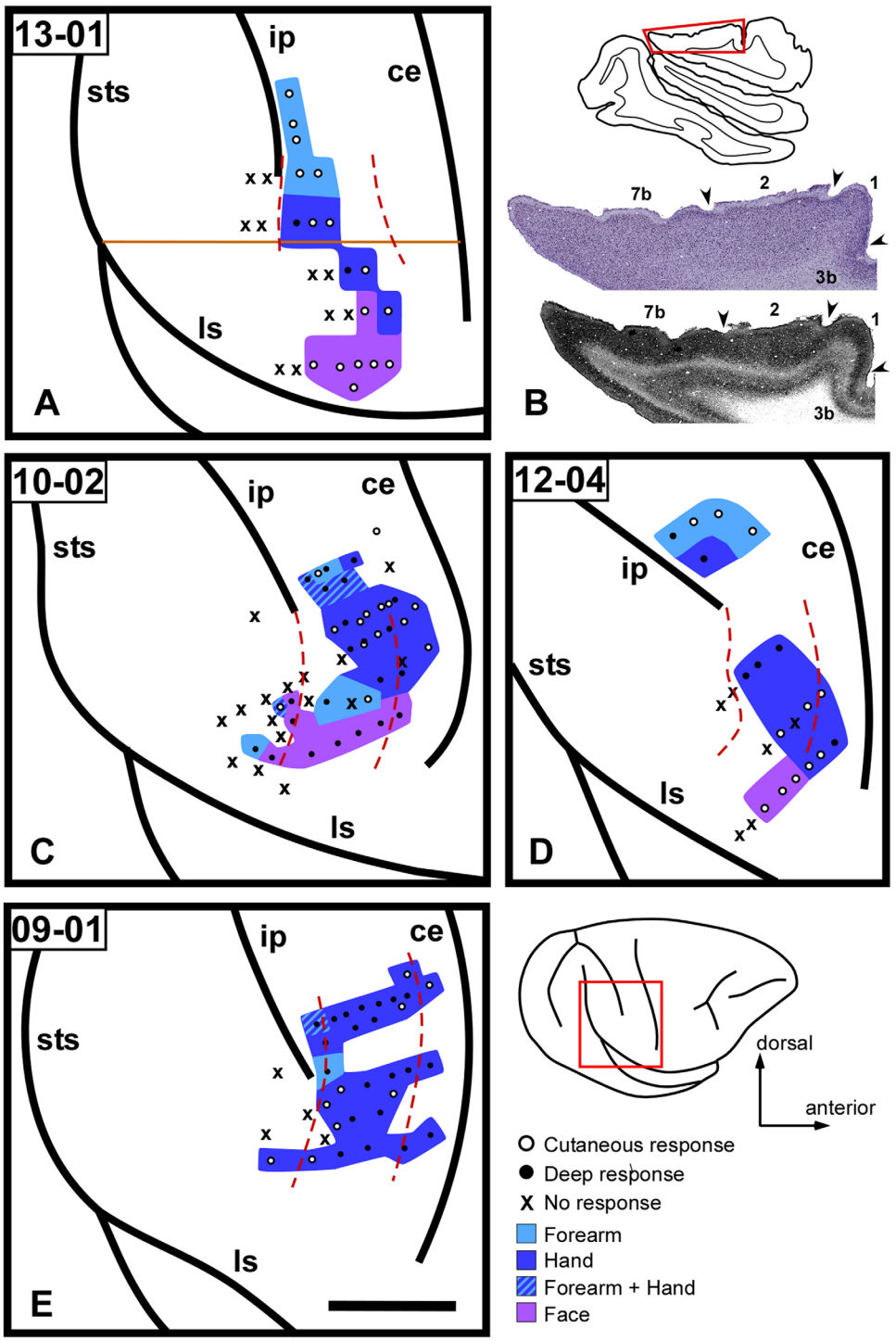

Figure 9. Somatosensory mapping of parietal cortex around and lateral to the tip of the intraparietal sulcus, obtained in four different cases **(A,C–E)**. This is the region where the transition from area 2 to area 7 is found. In anesthetized preparations, the border between areas 2 and 7 corresponds to the transition from a region responsive to cutaneous stimulation (area 2) to an unresponsive cortex (area 7). Filled and open black circles correspond to sites with neurons responsive to deep and superficial stimulation, respectively. Unresponsive sites are marked by x's. Red dashed lines represent the boundary between areas 7 and 2, or between areas 2 and 1 as estimated from architectonic analysis of the same cases. In the right inferior corner, a schematic drawing of a lateral view of the right hemisphere is illustrated. The red square depicts the region of the parietal cortex shown in A,C–E. **B:** Representative Nissl-stained and SMI-32 immunoreacted sections with indication of architectonic borders between areas 7b, 2, 1, and 3b (arrowheads). The approximate level of these sections is indicated by an orange horizontal line in A. ce = central sulcus; ip = intraparietal sulcus; sts = superior temporal sulcus; ls = lateral sulcus. Scale bar = 5 mm in E (applies to A,C–E). [Color figure can be viewed in the online issue, which is available at wileyonlinelibrary.com.]

The high-magnification micrographs used to characterize the different cortical areas under study (Figs. 4, 7, 8) were obtained from sections far from the lateral convexity of the cortex (Figs. 2B, 5B). Additionally, comparison between areas was mostly done considering cortical areas present in a same section. Thus, although slight mediolateral differences between sections may be present in our material, architectonic distinction between different cortical areas was still very clear along different sections.

Comparison with macaques

The architectonic organization of the anterior parietal cortex and area 5 in macaque monkeys has been described by many authors (Powell and Mountcastle, 1959; Nelson et al., 1980; Pandya and Seltzer, 1982; Pons et al., 1985; Lewis et al., 1999; Lewis and Van Essen, 2000; Krubitzer et al., 2004). However, except for two relatively recent studies (Lewis et al., 1999; Lewis and Van Essen, 2000), the anatomical characterization of parietal areas focused mostly on cytoarchitecture revealed by Nissl-stained sections (Powell and Mountcastle, 1959; Nelson et al., 1980; Pandya and Seltzer, 1982; Pons et al., 1985; Krubitzer et al., 2004), whereas in our study we additionally used myelin stain and SMI-32-immunoreacted sections. Therefore, the comparison of our data with that obtained in macaques was somewhat limited. Nevertheless, we found a great similarity in the cortical architecture of the somatosensory cortex of cebus and macaque monkeys. This resemblance has been previously reported by other studies based on electrophysiological data and Nissl stain. In previous studies of the cebus parietal cortex, however, the cytoarchitectonic data was either not shown (Felleman et al., 1983), or just briefly described based on a low-magnification analysis (Padberg et al., 2007).

In regard to the spatial arrangement of cortical areas of the parietal cortex, cebus and macaque monkeys present some interesting differences. Relative to the position of the CS, areas 1, 3b, and especially 3a of cebus monkeys were found in a different location than that usually observed in macaques (Nelson et al., 1980; Pons et al., 1985; Lewis et al., 1999; Krubitzer et al., 2004). In the cebus monkey, the largest part of area 3a was located in the anterior bank of the CS, close to the anterior margin of this sulcus, and never in the fundus, as one would expect based on macaque data (Krubitzer et al., 2004). Surprisingly, despite the difference in the orientation of the IPS, the relative location of areas 2, 5d, and 5v was similar in macaque and cebus monkeys (Fig. 1C,D).

Lateral to the tip of the IPS, the border between areas 2 and 7b was identified by electrophysiological mapping using the same criteria as adopted by Pons et al. (1985). Following extensive somatosensory mapping of area 2 in anesthetized macaque monkeys, those authors showed that, lateral to the tip of IPS, cortex about 3–4 mm caudal from area 1 was unresponsive to somatic stimulation. They used this unresponsiveness as a criterion to delimit the caudal border of area 2. However, according to Pons et al. (1985) the cortical region caudal to area 2 was not easily distinguished from area 2 proper based on architectonic analysis of Nissl-stained sections. Therefore, Pons et al. (1985) were not able to estimate an anatomical caudal border of area 2. In our material, we confirmed the difficulty to delimit the caudal border of area 2 based solely on Nissl stain. However, associating SMI-32 immunoreactivity and myelin stain, this cortical boundary was reliably estimated, correlating well with the electrophysiological border, although a few responsive sites were observed posterior to the caudal border of area 2, in the expected location of area 7b (Fig. 9).

The boundary between areas 2 and 7b/PF in macaques was also explored by Gregoriou et al. (2006). In that study the authors described the architecture of different sectors in the inferior parietal cortex of macaque monkeys. The rostral border of area 7b/PF with area 2 was identified by cyto- and myeloarchitectonic criteria and was in a relatively similar location to what we observed in cebus monkey. According to the authors, area 2 (in macaque) presented a markedly higher cellular density than area 7b/PF, especially in layers 3 and 4. This description somehow matches what we saw in the cebus monkey, in which area 2 clearly presented a well-developed layer 3 in both SMI-32 immunohistochemistry (Fig. 9B) and Nissl stain (data not shown). Unfortunately, Gregoriou et al. (2006) did not show high-magnification data from area 2, so we could not do a more detailed comparison.

Subdivisions of area 5 and possible parcellation of area 2

Current electrophysiological and cytoarchitectonic studies of the macaque monkey support the established notion that the anterior parietal cortex can be subdivided in the cortical areas 3a, 3b, 1, and 2. The organization of area 5, however, is more disputed. Different authors diverge regarding anatomical and functional subdivisions and its respective nomenclatures. Based on myelin and Nissl stains, and on corticocortical connectivity, Pandya and Seltzer (1982) divided area 5 of Brodmann into three anatomically different sectors.

Using the same terminology as von Economo (1929), those authors divided area 5 into area PE, situated in the superior parietal cortex, area PE caudal (PEc), located mediocaudally to the first, and area PEa, located in the entire mediolateral extent of the dorsal bank of IPS. Later, based on corticocortical connectivity, area PEa was subdivided into MIP (Colby et al., 1988), in the medial portion of the superior bank of the IPS, and PE intraparietal (PEip; Matelli et al., 1998), in the remainder of the superior bank, rostral to MIP. Alternatively, other authors slightly modified the original nomenclature proposed by Brodmann, dividing area 5 into two functionally and/or anatomically different sectors. Based on SMI-32 immunoreactivity, myelo- and cytoarchitecture, Lewis and Van Essen (2000) proposed the subdivision of area 5 of Brodmann into areas 5-dorsal (5d) and 5-ventral (5v). The first is located in the posterior portion of the postcentral gyrus and in the dorsal edge of the IPS, while area 5v is located in the dorsal bank of IPS. Recently, after mapping the topographic organization of the lateral portion of area 5, Seelke et al. (2012) proposed that this cortical region, termed 5L, could be functionally distinguished from medial portions (the "medial IPS regions"). This parcellation was further supported by Cooke et al. (2013) based on differences in the corticocortical connectivity between medial and lateral portions of area 5, which were then termed 5M and 5L, respectively.

In cebus monkey, area 5 can be subdivided into three sectors, areas 5d and 5v (see Fig. 1), plus MIP (in the medial portion of the anterior bank of IPS, Figs. 1, 2A–C, 3A–C). Our analyses did not extend to the region medial and caudal to area 5d. Thus, additional subdivisions of area 5 in the expected location of area PEc (Pandya and Seltzer, 1982; Breveglieri et al., 2006; Bakola et al., 2010) still need to be investigated. Although we adopted the nomenclature used by Lewis and Van Essen, (2000), area 5v in cebus monkey was actually located not just ventrally but also laterally to area 5d (Fig. 1D). Thus, the spatial arrangement of the parietal areas that we observed in the cebus monkey was somewhat in between that of Lewis and Van Essen (2000; 5d and 5v) and what was proposed by Seelke et al. (2012) and Cooke et al. (2013; 5M and 5L) for macaque monkeys.

Interestingly, similar to area 5, which can be subdivided in dorsal (5d) and ventral (5v) sectors, the medial and lateral portions of area 2 in case 13-01 were differentially immunolabeled for SMI-32 (compare Fig. 2A,B with 2E). The infragranular layers of the lateral sector of area 2, especially in the region corresponding to forearm and hand representations, is more intensely immunoreactive for SMI-32 than those in the medial sector. Although area 2 has been classically described as a unique area running parallel to area 1 in the postcentral gyrus (Nelson et al., 1980; Pons et al., 1985; Pons and Kaas, 1986; Padberg et al., 2007), this difference in immunoreactivity in area 2 may be related to functionally different sectors. For instance, long-term microstimulation in the lateral portion of area 2 in macaques, close to the tip of IPS, evoke complex grasping movements, whereas no movement is observed after microstimulation in more medial portions (Gharbawie et al., 2011). On the other hand, neurons in the medial portion of area 2 respond to actively and passively generated limb movements (London and Miller, 2013), suggesting their involvement in the sensorimotor integration for reaching. Therefore, architectonic differences between medial and lateral portions of area 2 could reflect segregated specializations concerned with different behaviors (e.g., grasping and reaching). Further investigation using anatomical tools like SMI-32 immunohistochemistry and anatomical tracers, associated with behavioral/electrophysiological paradigms, must be done in order to better explore possible functional and anatomical parcellation of area 2.

Somatosensory areas and manual behaviors

In primates, each of the somatosensory areas has an enlarged representation of the forelimb (Degnan et al., 1979; Nelson et al., 1980; Felleman et al., 1983; Pons et al., 1985; Padberg et al., 2007; Seelke et al., 2012), which suggests that they all have some contribution to the integration of somatosensory inputs for manual behaviors. During primate evolution, the increment of new somatosensory areas providing additional computational capability to the somatomotor circuit was certainly a necessary step for development of fine manual control. As previously discussed, cebus monkeys stand out from other New World primates by their ability to perform fine hand movements and to manufacture and use tools (Moura and Lee, 2004; Spinozzi et al., 2004, 2007; Schrauf et al., 2008; Mannu and Ottoni, 2009; Visalberghi et al., 2009; Manrique et al., 2011). Therefore, it was not a surprise to find a relatively complex somatosensory cortex in this primate (see above).

Our data confirm and extend previous findings in cebus monkeys (Padberg et al., 2007) by demonstrating that, besides a well-developed cortical area 2, these animals also have a complex area 5, which can be further subdivided into at least three different architectonic sectors. Similar complexity of the somatosensory cortex is observed in macaques and humans (Geyer et al., 1997; Scheperjans et al., 2005), but not in other New World monkeys (for review, see Padberg et al., 2005). For instance, in titi monkeys, posterior to area

3a and 3b there is only an area 1 bordering a poorly developed area 5 (Padberg et al., 2005). Padberg et al. (2007) proposed that the emergence of area 2 and a well-developed area 5 during primate evolution could be linked to increments in manual abilities.

In both macaques and cebus monkeys, area 2 is still part of the anterior parietal cortex, and it is dominated by the hand and face representations (Pons et al., 1985; Padberg et al., 2007). Neuronal firing in area 2 is modulated by actively and passively generated limb movements (Burbaud et al., 1991; London and Miller, 2013), and during contact and grasping of objects (Debowy et al., 2001; Gardner et al., 2007). Long-train intracortical microstimulation in area 2 can evoke complex movements of grasping (Gharbawie et al., 2011). In addition, chemical inactivation of the hand region in area 2 can disrupt the fine coordination of fingers during grasping behaviors (Hikosaka et al., 1985).

In contrast, area 5 is considered part of the posterior parietal cortex, and it is almost exclusively dominated by the forelimb representation (Padberg et al., 2007; Seelke et al., 2012). Neuronal firing in area 5 is modulated not only during grasping, but also during object approach, that precedes grasping, when the hand is preshaped for object contact (Debowy et al., 2001; Gardner et al., 2007). The firing modulation that occurs during this phase can be correlated with the object's physical properties, like shape and size (Chen et al., 2009). Neuronal firing properties suggest that area 5 is involved in coding body- and shoulder-centered coordinates (Ferraina and Bianchi, 1994; Lacquaniti et al., 1995) necessary for the first reaching movement within a preestablished sequence of arm movements (Li and Cui, 2013). Lesions in area 5 can impair or even prevent the execution of manual tasks (Padberg et al., 2010), including misreaching in the dark (but not in the light) (Rushworth et al., 1997), clearly suggesting a role of area 5 in somatomotor integration. Connectional studies showed that sectors of area 5 are connected with all other somatosensory areas as well as with the primary motor area and with ventral and dorsal premotor sectors (Gharbawie et al., 2011). Area 5 is also involved in the incorporation of tools in the body scheme. The receptive fields of neurons in regions corresponding to area 5 change depending on if the monkey is using a hand or a tool (e.g., rake) to reach and grasp an object (Iriki et al., 1996).

Taken together, the relatively complex somatosensory cortex of the cebus monkey, characterized by numerous cortical fields, including the presence of an area 2 and a well-developed area 5, should be one of the key features to endow these animals with the ability to perform outstanding manual behaviors. The specific role of each architectonic subdivision, however, is still unclear. In the present study we showed that clear anatomical boundaries provide a reliable substrate for the parcellation of the somatosensory cortex. Hopefully, future studies aiming to unveil the specific contribution of these cortical areas in different manual and tool-using behaviors will be able to provide the functional correlation necessary to further understand the organization of the parietal cortex.

ACKNOWLEDGMENTS

This study is part of the Ph.D. thesis of AMO, who was under the Graduate Program in Biological Sciences – Physiology of the Federal University of Rio de Janeiro (UFRJ, http://www.biof.ufrj.br/en/node/628). As a PhD student, AMO was awarded a CNPq scholarship (proc. #141614/2012-9).

CONFLICT OF INTEREST

We declare that there is no conflict of interest, either financial, personal, or other relationships with other people or organizations within 3 years of beginning the submitted work that could inappropriately influence the results or interpretation of the data of the article.

AUTHOR ROLES

All authors had full access to all the data in the study and take responsibility for the integrity of the data and the accuracy of the data analysis. Study concept and design: AMO, JGF. Acquisition of data: AMO, MLNS, NBK, REBN, JGF. Analysis and interpretation of data: AMO, MLNS, NBK, JGF, RG. Drafting of the article: AMO. Critical revision of the article for important intellectual content: AMO, REBN, RG, JGF. Funding obtained by RG and JGF. Study supervision: JGF and RG.

LITERATURE CITED

Bakola S, Gamberini M, Passarelli L, Fattori P, Galletti C. 2010. Cortical connections of parietal field PEc in the macaque: linking vision and somatic sensation for the control of limb action. Cereb Cortex 20:2592–2604.

Bakola S, Passarelli L, Gamberini M, Fattori P, Galletti C. 2013. Cortical connectivity suggests a role in limb coordination for macaque area PE of the superior parietal cortex. J Neurosci 33:6648–6658.

Boire D, Desgent S, Matteau I, Ptito M. 2005. Regional analysis of neurofilament protein immunoreactivity in the hamster's cortex. J Chem Neuroanat 29:193–208.

Breveglieri R, Galletti C, Gamberini M, Passarelli L, Fattori P. 2006. Somatosensory cells in area PEc of macaque posterior parietal cortex. J Neurosci 26:3679–3684.

Brodmann K. 1909. Vergleichende Lokalisationslehre der Grosshirnrinde in ihren Prinzipien Dargestellt auf Grund des Zellenbaues. Leipzig, Germany: Barth.

Budde MD, Annese J. 2013. Quantification of anisotropy and fiber orientation in human brain histological sections. Front Integr Neurosci 7:3.

Burbaud P, Doegle C, Gross C, Bioulac B. 1991. A quantitative study of neuronal discharge in areas 5, 2, and 4 of the monkey during fast arm movements. J Neurophysiol 66: 429–443.

Campbell MJ, Morrison JH. 1989. Monoclonal antibody to neurofilament protein (SMI-32) labels a subpopulation of pyramidal neurons in the human and monkey neocortex. J Comp Neurol 282:191–205.

Chen J, Reitzen SD, Kohlenstein JB, Gardner EP. 2009. Neural representation of hand kinematics during prehension in posterior parietal cortex of the macaque monkey. J Neurophysiol 102:3310–3328.

Colby CL, Gattass R, Olson CR, Gross CG. 1988. Topographical organization of cortical afferents to extrastriate visual area PO in the macaque: a dual tracer study. J Comp Neurol 269:392–413.

Cooke DF, Padberg J, Cerkevich CM, Kaas JH, Krubitzer. Corticocortical connections of area 5 in macaque monkeys support the existence of functionally distinct medial and lateral regions. Program No. 551.09.2013 Neuroscience Meeting Planner. San Diego, CA: Society for Neuroscience, 2013. Online.

Cruz-Rizzolo RJ, De Lima MAX, Ervolino E, de Oliveira JA, Casatti CA. 2011. Cyto-, myelo- and chemoarchitecture of the prefrontal cortex of the cebus monkey. BMC Neurosci 12:6.

Debowy DJ, Ghosh S, Gardner EP, Ro JY. 2001. Comparison of neuronal firing rates in somatosensory and posterior parietal cortex during prehension. Exp Brain Res 137:269–291.

Degnan KJ, Lederis K, Rogers NL, Sutherland EW, Newman EV. 1979. Multiple representation of the body within the primary somatosensory cortex of primates. Science 204: 1977–1979.

Dias IA, Bahia CP, Franca JG, Houzel JC, Lent R, Mayer AO, Santiago LF, Silveira LCL, Picanço-Diniz CW, Pereira A. 2014. Topography and architecture of visual and somatosensory areas of the agouti. J Comp Neurol 522:2576–2593.

Felleman DJ, Nelson RJ, Sur M, Brook S. 1983. Representations of the body surface in areas 3b and 1 of postcentral parietal cortex of cebus monkeys. Brain Res 268:15–26.

Ferraina S, Bianchi L. 1994. Posterior parietal cortex: functional properties of neurons in area 5 during an instructed-delay reaching task within different parts of space. Exp Brain Res 99:175–178.

Gardner EP, Ro JY, Babu KS, Ghosh S. 2007. Neurophysiology of prehension. II. Response diversity in primary somatosensory (S-I) and motor (M-I) cortices. J Neurophysiol 97: 1656–1670.

Geyer S, Schleicher A, Zilles K. 1997. The somatosensory cortex of human: cytoarchitecture and regional distributions of receptor-binding sites. Neuroimage 6:27–45.

Gharbawie OA, Stepniewska I, Qi H, Kaas JH. 2011. Multiple parietal-frontal pathways mediate grasping in macaque monkeys. J Neurosci 31:11660–11677.

Gregoriou GG, Borra E, Matelli M, Luppino G. 2006. Architectonic organization of the inferior parietal convexity of the macaque monkey. J Comp Neurol 496:422–451.

Gumert MD, Malaivijitnond S. 2013. Long-tailed macaques select mass of stone tools according to food type Long-tailed macaques select mass of stone tools according to food type. Philos Trans R Soc 368:1–13.

Gumert MD, Kluck M, Malaivijitnond S. 2009. The physical characteristics and usage patterns of stone axe and pounding hammers used by long-tailed macaques in the Andaman Sea region of Thailand. Am J Primatol 71:594–608.

Hikosaka O, Tanaka M, Sakamoto M, Iwamura Y. 1985. Deficits in manipulative behaviors induced by local injections of muscimol in the first somatosensory cortex of the conscious monkey. Brain Res 325:375–380.

Hof PR, Morrison JH. 1995. Neurofilament protein defines regional patterns of cortical organization in the macaque monkey visual system: a quantitative immunohistochemical analysis. J Comp Neurol 352:161–186.

Hutchins B, Weber JT. 1983. A rapid myelin stain for frozen sections: modification of the Heidenhain procedure. J Neurosci Methods 7:289–294.

Iriki A, Tanaka M, Iwamura Y. 1996. Coding of modified body schema during tool use by macaque postcentral neurones. NeuroReport 7:2325–2330.

Jones EG, Coulter JD, Hendry SH. 1978. Intracortical connectivity of architectonic fields in the somatic sensory, motor and parietal cortex of monkeys. J Comp Neurol 181:291–347.

Krubitzer L, Huffman KJ, Disbrow E, Recanzone G. 2004. Organization of area 3a in macaque monkeys: contributions to the cortical phenotype. J Comp Neurol 471:97–111.

Lacquaniti F, Guigon E, Bianchi L, Ferraina S, Caminiti R. 1995. Representing spatial information for limb movement: role of area 5 in the monkey. Cereb Cortex 5: 391–409.

Lewis JW, Van Essen DC. 2000. Mapping of architectonic subdivisions in the macaque monkey, with emphasis on parieto-occipital cortex. J Comp Neurol 428:79–111.

Lewis JW, Burton H, Van Essen DC. 1999. Anatomical evidence for the posterior boundary of area 2 in the macaque monkey. Somatosens Mot Res 16:382–390.

Li Y, Cui H. 2013. Dorsal parietal area 5 encodes immediate reach in sequential arm movements. J Neurosci 33: 14455–14465.

London BM, Miller LE. 2013. Responses of somatosensory area 2 neurons to actively and passively generated limb movements. J Neurophysiol 109:1505–1513.

Malaivijitnond S, Lekprayoon C, Tandavanittj N, Panha S, Cheewatham C, Hamada Y. 2007. Stone-tool usage by Thai long-tailed macaques (Macaca fascicularis). Am J Primatol 233:227–233.

Mannu M, Ottoni EB. 2009. The enhanced tool-kit of two groups of wild bearded capuchin monkeys in the Caatinga: tool making, associative use, and secondary tools. Am J Primatol 71:242–251.

Manrique HM, Sabbatini G, Call J, Visalberghi E. 2011. Tool choice on the basis of rigidity in capuchin monkeys. Anim Cogn 14:775–786.

Matelli M, Govoni P, Galletti C, Kutz DF, Luppino G. 1998. Superior area 6 afferents from the superior parietal lobule in the macaque monkey. J Comp Neurol 402:327–352.

Moura A, Lee P. 2004. Capuchin stone tool use in Caatinga dry forest. Science 306:1909.

Nelson RJ, Sur M, Felleman DJ, Kaas JH. 1980. Representations of the body surface in postcentral parietal cortex of Macaca fascicularis. J Comp Neurol 192:611–643.

Padberg J, Disbrow E, Krubitzer L. 2005. The organization and connections of anterior and posterior parietal cortex in titi monkeys: do New World monkeys have an area 2? Cereb Cortex 15:1938–1963.

Padberg J, Franca JG, Cooke DF, Soares JGM, Rosa MGP, Fiorani M, Gattass R, Krubitzer L. 2007. Parallel evolution of cortical areas involved in skilled hand use. J Neurosci 27:10106–10115.

Pandya DN, Seltzer B. 1982. Intrinsic connections and architectonics of posterior parietal cortex in the rhesus monkey. J Comp Neurol 204:196–210.

Pons TP, Kaas JH. 1986. Corticocortical connections of area 2 of somatosensory cortex in macaque monkeys: a

correlative anatomical and electrophysiological study. J Comp Neurol 248:313–335.
Pons TP, Garraghty PE, Cusick CG, Kaas JH. 1985. The somatotopic organization of area 2 in macaque monkeys. J Comp Neurol 241:445–466.
Powell TPS, Mountcastle VB. 1959. The cytoarchitecture of the postcentral gyrus of the monkey *Macaca mulatta*. Bull Johns Hopkins Hosp. 105:108–131.
Rozzi S, Ferrari PF, Bonini L, Rizzolatti G, Fogassi L. 2008. Functional organization of inferior parietal lobule convexity in the macaque monkey: electrophysiological characterization of motor, sensory and mirror responses and their correlation with cytoarchitectonic areas. Eur J Neurosci 28:1569–1588.
Rushworth MFS, Nixon PD, Passingham RE. 1997. Parietal cortex and movement. Exp Brain Res 117:311–323.
Scheperjans F, Grefkes C, Palomero-Gallagher N, Schleicher A, Zilles K. 2005. Subdivisions of human parietal area 5 revealed by quantitative receptor autoradiography: a parietal region between motor, somatosensory, and cingulate cortical areas. Neuroimage 25:975–992.
Schrauf C, Huber L, Visalberghi E. 2008. Do capuchin monkeys use weight to select hammer tools? Anim Cogn 11: 413–422.
Seelke AMH, Padberg JJ, Disbrow E, Purnell SM, Recanzone G, Krubitzer L. 2012. Topographic maps within Brodmann's area 5 of macaque monkeys. Cereb Cortex 22:1834–1850.
Soares JGM, Rosado De Castro PH, Fiorani M, Nascimento-Silva S, Gattass R. 2008. Distribution of neurofilament proteins in the lateral geniculate nucleus, primary visual cortex, and area MT of adult cebus monkeys. J Comp Neurol 508:605–614.
Spinozzi G, Truppa V, Laganà T. 2004. Grasping behavior in tufted capuchin monkeys (Cebus apella): grip types and manual laterality for picking up a small food item. Am J Phys Anthropol 125:30–41.
Spinozzi G, Truppa V, Laganà T. 2007. Hand use by tufted capuchins (*Cebus apella*) to extract a small food item from a tube: digit movements, hand preference, and performance. Am J Primatol 352:336–352.
Sternberger LA, Sternberger NH. 1983. Monoclonal antibodies distinguish phosphorylated and nonphosphorylated forms of neurofilaments in situ. Proc Natl Acad Sci U S A 80: 6126–6130.
Van der Gucht E, Hof PR, Van Brussel L, Burnat K, Arckens L. 2007. Neurofilament protein and neuronal activity markers define regional architectonic parcellation in the mouse visual cortex. Cereb Cortex 17:2805–2819.
Van Essen DC, Drury H, Dickson J, Harwell J, Hanlon D, Anderson CH. 2001. An integrated software suite for surface-based analyses of cerebral cortex. J Am Med Inform Assoc 8:443–459.
Visalberghi E, Addessi E, Truppa V, Spagnoletti N, Ottoni E, Izar P, Fragaszy D. 2009. Selection of effective stone tools by wild bearded capuchin monkeys. Curr Biol 19:213–217.
Vogt C, Vogt O. 1919. Ergebnisse unserer Hirnfomhung. Viertemitteilung: die physiologische bedeutung der architektonischen rin- denreizungen. J Psychol Neurol 25:277–462.
von Bonin G, Bailey P. 1947. The neocortex of macaca mulatta. Urbana, IL: University of Illinois.
von Economo C. 1929. The cytoarchitectonics of the human cerebral cortex. London: Oxford University Press.
von Economo C, Hoskinas GN. 1925. Die Cytoarchitektonik der Hirninde des erwachsenen Menschen. Berlin: Springer.